Electronic Supplementary Information

Activating the Neutral pH Photozymatic Activity of g-C_3N_4 Nanosheet through Post-Synthetic Incorporation of Pt

Xue Li,[a] Xianming Li,[a] Qian Chen,[a] Junbo Chen,*[,a] Peng Wu*[, a, b]

[a] Analytical & Testing Center, State Key Laboratory of Hydraulics and Mountain River Engineering, Sichuan University, Chengdu 610064, China

[b] School of Chemistry and Chemical Engineering, Henan Normal University, Xinxiang, 453007, China.

***Corresponding authors' E-mail:** junbochen@scu.edu.cn (Junbo Chen), wupeng@scu.edu.cn (Peng Wu)

Table of Contents

Section 1. Experimental Section

1.1 Reagents

The detailed information of the reagents was given in Table S1.

Table S1. The Reagent information in this work.

Name	CAS No.	Specification	Supplier
$H_2PtCl_6 \cdot 6H_2O$	18497-13-7	ACS	Sigma-Aldrich, Shanghai, China
Folin & Ciocalteu reagent (2 N)	/	/	Sigma-Aldrich, Shanghai, China
Carbon nitride ethanol-water dispersion	/	/	XFNANO, Nanjing, China
3, 3', 5, 5'-tetramethylbenzidine	54827-17-7	98%	Aladdin, Shanghai, China
Dimethyl sulfoxide	67-68-5	≥ 99.8%	Aladdin, Shanghai, China
(-)-Epigallocatechin gallate	989-51-5	98%	Aladdin, Shanghai, China
(±)-Catechin hydrate (CT)	7295-85-4	96%	Aladdin, Shanghai, China
Rutin (RT)	153-18-4	95%	Aladdin, Shanghai, China
Quercetin (QR)	117-39-5	95%	Aladdin, Shanghai, China
Ascorbic acid (AA)	89924-69-6	≥ 99.7%	Kelong, Chengdu, China
Caffeic acid (CA)	331-39-5	98%	Aladdin, Shanghai, China
Chlorogenic acid (CHA)	327-97-9	98%	Aladdin, Shanghai, China
Gallic acid (GA)	149-91-7	99%	Aladdin, Shanghai, China
$HAuCl_4$	16961-25-4	99.9%	Aladdin, Shanghai, China
K_2PdCl_6	16919-73-6	≥26.3% (Pd)	Aladdin, Shanghai, China

Ultra-pure water obtained from a Millipore water purification system (≥18.2 MΩ, Milli-Q, Millipore) was used throughout this work.

1.2 Instruments

All the instrumental information used for characterizations were given in Table S1.

Table S2. The instrumental information used in this work.

Characterization items	Instrument model	Manufacturer
Absorption spectra	Lambda-365 spectrophotometer	Perkin Elmer, USA
Fluorescence spectra	FluoroMax-4P spectrofluorometer	Horiba Scientific, USA
Fluorescence/ Phosphorescence lifetime	Fluolog-3 Ex: SpectraLED (355 nm, S-355), DeltaDiode (320 nm, DD-320)	Horiba Jobin Yvon, USA
EPR	EMXplus-10/12	Bruker, Switzerland
TEM	Tecnai G2 F20 S-TWIN Acceleration voltage: 200 kV	FEI, USA
XPS	AXIS Ultra DLD Excitation: Al-Kα X-ray	Kratos, Japan
Zeta potential	Zetasizer Nano ZS	Malvern, England
Pt contents	5100 SVDV ICP-OES	Agilent, USA

1.3 Synthesis of Pt@CNNS

CNNS was obtained from XFNANO, Nanjing, China. Specifically, g-C3N4 was produced by thermal polymerization of dicyandiamide at 550 °C (ramp rate of ~5 ºC/min) for 4 h under nitrogen atmosphere. After cooling down, the yellowish product was collected and washed with distilled water to remove the residual ammonium. CNNS was obtained through exfoliating of g-C_3N_4 in ethanol.

Pt@CNNS was prepared via a simple post-synthetic strategy. Briefly, 5 mL carbon nitride ethanol-water dispersion was washed by water, then re-dissolved in water. After ultra-sonication for 30 minutes, mixing 2.5 mL H_2PtCl_6 (10 mM) in carbon nitride water solution. Then, the mixture was heated at 60 ºC for 6 hours. Finally, the resulting orange-yellow dispersion was washed with ethanol and water for six times each. For

Au@CNNS and Pd@CNNS, the synthesis routes were similar to that of Pt@CNNS, except $HAuCl_4$ and K_2PdCl_6 was explored.

1.4 Photozymatic activity and steady-state kinetic analysis of CNNS and Pt@CNNS

The photozymatic activity of CNNS and Pt@CNNS were evaluated according to the previous work.[1] The experiments were conducted in sodium acetate buffer (20 mM, pH 4.0 or pH 7.0) containing Pt@CNNS (0.05 mg mL^{-1}) and TMB (0.8 mM, DMSO). Then the mixture was irradiated by LED (3V, 3W) for 100 s. The absorption spectra of the reaction solution were measured after centrifugation at 12000 rpm for 5 minutes. The experimental procedures under alkaline conditions were the same as the above, except that the medium was sodium acetate containing sodium hydroxide (100 mM).

The steady-state kinetic analysis was carried out. In a typical procedure, TMB was added in sodium acetate buffer (20 mM, pH 4.0 or pH 7.0) containing Pt@CNNS (0.05 mg mL^{-1}) by changing the concentration of TMB (0.1-1.0 M), then the absorbance at 652 nm was measured using UV-vis spectrophotometer after 3 s of each irradiation. Additionally, the kinetic parameters were calculated according to the Michaelis-Menten equation as follows:

$$\frac{1}{V} = \left(\frac{K_m}{V_{max}}\right) * \left(\frac{1}{[S]}\right) + \frac{1}{V_{max}}$$

Where K_m is the Michaelis constant, V_{max} is the maximum reaction velocity, and [S] is the TMB concentration.

1.5 Absorption of Pt@CNNS and CNNS with TMB

For the typical absorption process, sodium acetate buffer (20 mM, pH = 7.0) containing Pt@CNNS or CNNS (0.05 mg mL^{-1}) and TMB (0.8 mM, DMSO) were mixed to 2-mL centrifugation tube and then diluted to 1 mL by water. After incubated 1min, centrifugation at 12000 rpm for 30 minutes. At last, the absorbance of supernatants was detected. As for control, TMB without photozyme was the blank group.

1.6 ROS characterization

For ROS scavenging, the corresponding ROS-specific scavengers, namely superoxide dismutase (SOD) for $\cdot O_2^-$, D-tryptophan for $^1O_2$, catalase for H_2O_2, and mannite for ·OH, were used.[2] The concentrations for the above scavengers were: SOD, 800 U; D-tryptophan, 4.9 mM; catalase, 150 U; mannite, 10.0 mM. The experimental procedures were the same as the above (photozymatic activity), except that the absorbance was measured in the presence of the scavengers.

For EPR measurements, TEMP and DMPO (100 mM) were employed as the spin traps for $^1O_2$ and $\cdot O_2^-$, respectively. After irradiation for 10 min, the EPR spectra were recorded.

For ·OH measurement, terephthalate (6 mM) incubated with Pt@CNNS under blue LED irradiation for 30 minutes.

1.7 Assessing the antioxidants in alleviating photozymatic activity

The colorimetric system responded to the main antioxidants in tea leaves at both neutral and acidic pH levels. For the eight typical antioxidants in tea, including (-)-Epigallocatechin gallate (EGCG), (±)-Catechin hydrate (CT), Gallic acid (GA), Ascorbic acid (AA), Chlorogenic acid (CHA), Caffeic acid (CA), Quercetin (QR), Rutin, were explored. In a typical procedure, 20 μM GA was added in sodium acetate buffer (20 mM, pH 4.0 or pH 7.0) containing Pt@CNNS (0.05 mg/mL) and TMB (0.8 mM, DMSO). After irradiation for 100 s, the absorbance at 65 nm was recorded.

1.8 Evaluation antioxidants capacities in tea samples at neutral pH

Tea was bought from the local market. Firstly, dry leaves (0.05 g) of each tea were suspended in 25 ml water at different temperature. Then the tea was kept for 15 min (at different temperature 20 ºC -100 ºC) or 1 min (at 100 ºC). Finally, the tea extracts were filtered with 0.22 μm membrane. The resultant samples were stored at 4 ºC refrigerator.

The antioxidant capacity was evaluated by using the standard curve method. The 100-fold diluted tea samples were added into sodium acetate buffer (20 mM, pH 7.0) containing TMB (0.8 mM, DMSO), Pt@CNNS (0.05 mg mL^{-1}) and the absorbance at 652 nm measured. As for control experiments, classical spectroscopic Folin-Ciocalteu method was also introduced to evaluate total antioxidants in tea. Briefly to the volume of 1 mL GA solution or practical sample solution, 5 mL of F-C reagent (10%, v/v) was added. Then, after 5 minutes, 4 mL of Na_2CO_3 (7.5%, v/v) was mixed with the above solution and the mixture was incubated at 25 ºC for 1 hour. The reacted system was detected by a UV-vis spectrophotometer and the absorbance was recorded at 765 nm.

Section 2. Materials characterizations

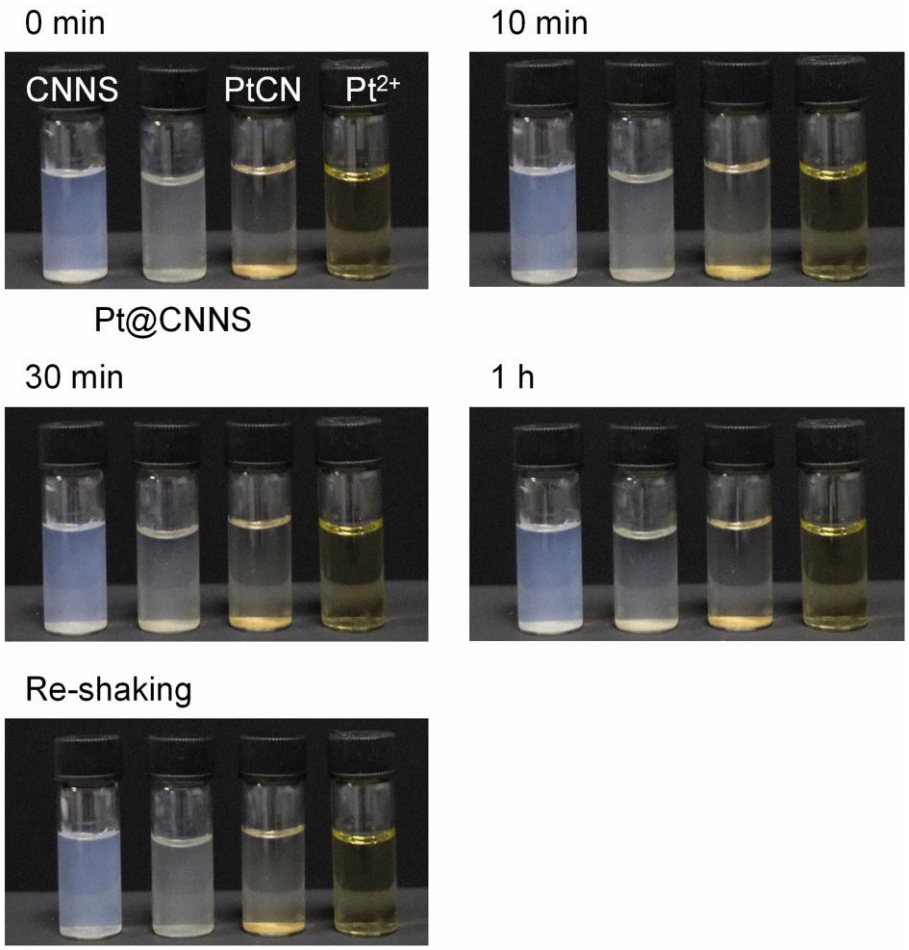

Figure S1 Comparison of the dispersion of materials synthesized by pre-doping (PtCN) and post-doping (Pt@CNNS).

Notes: The pre-doped PtCN could not be homogeneously dispersed, while the post-doped Pt@CNNS started to show a small amount of precipitation after one hour and was homogeneously redispersed after shaking.

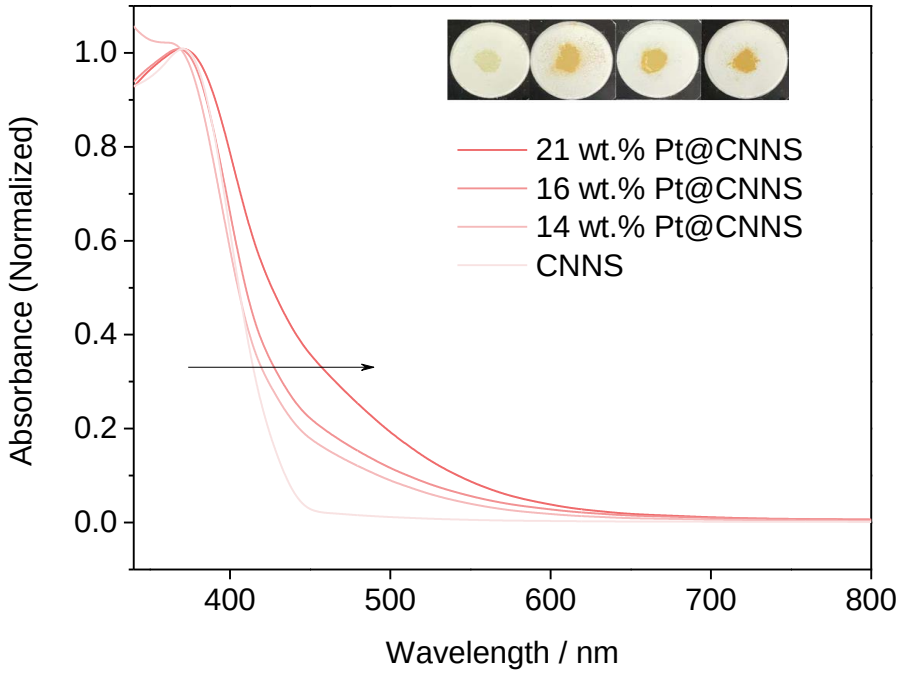

Figure S2. The UV-vis diffused reflectance spectra of CNNS and Pt@CNNS.

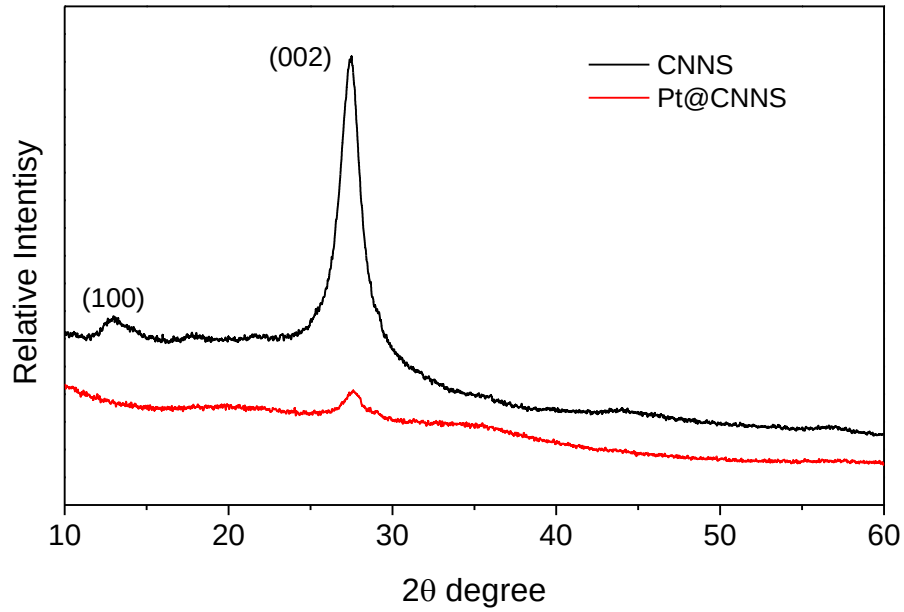

Figure S3. The XRD patterns of CNNS and Pt@CNNS.

Notes: Compared with CNNS, the peak shape was broadened, accompanied with sharply decreased peak intensity, clearly demonstrating that the layered structure of CNNS was perturbed upon Pt incorporation.

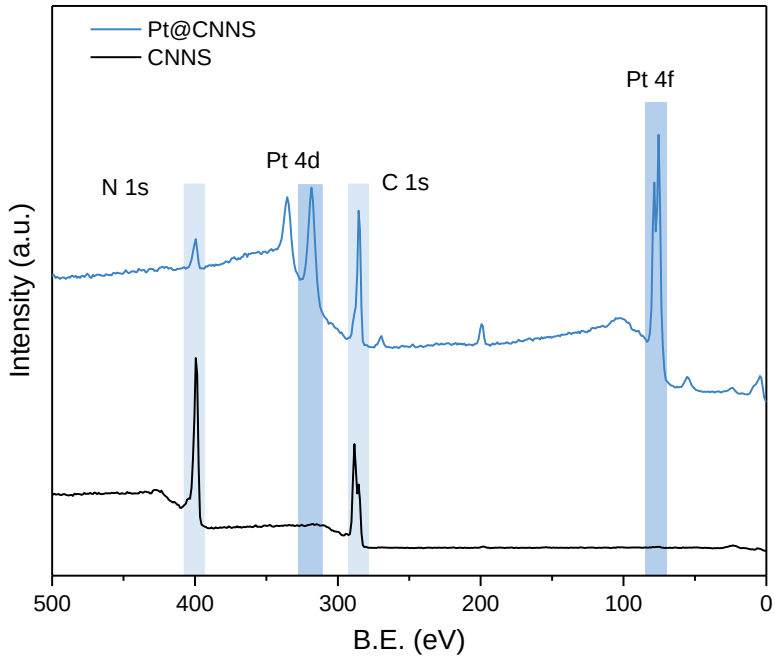

Figure S4. Full spectra XPS of CNNS and Pt@CNNS.

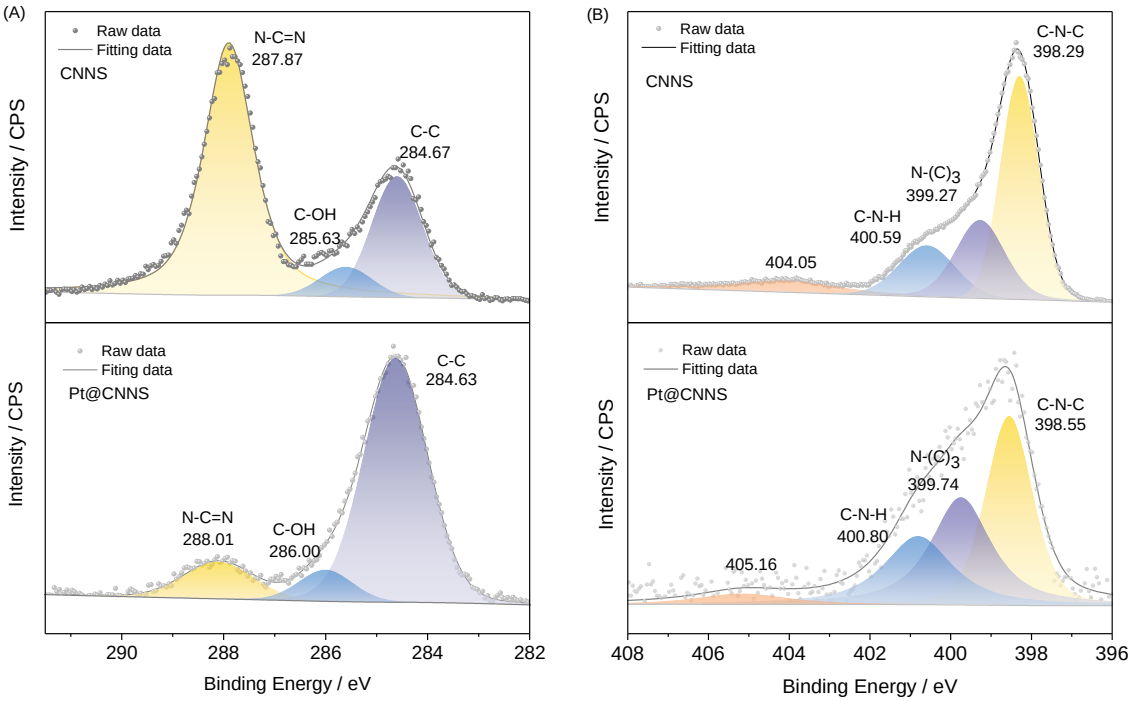

Figure S5. The high resolution XPS profiles of (A) C 1s and (B) N 1s.

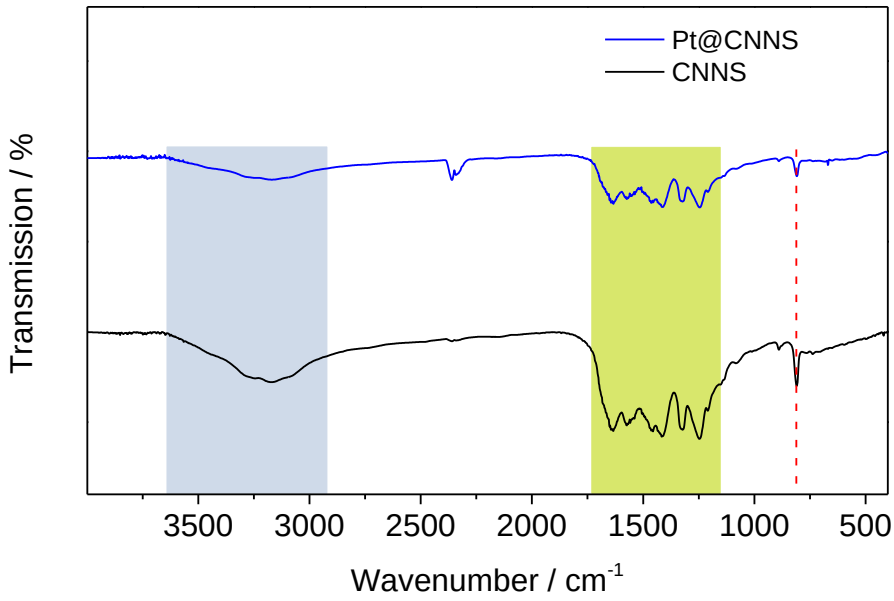

Figure S6. The FTIR spectra of CNNS and Pt@CNNS.

Notes: The bonding of carbon and nitrogen in the CNNS and Pt@CNNS was analyzed through FTIR spectra. They exhibited several major bands centered at about 3180 cm^{-1}, 1160-1730 cm^{-1} and 806 cm^{-1}. The broad 3180 cm^{-1} band can be attributed to the stretching vibration of N–H groups and the stretching modes in the 1200-1700 cm^{-1} range were typical for aromatic C-N heterocycles. In addition, the characteristic breathing mode of the triazine unit is observed at 806 cm^{-1}.[3] The intensity of these peaks decreases with Pt doping, suggesting that CNNS contains numerous triazine rings that comprise sp^2 C-N bonds such as N=C-N and C-N=C.[4]

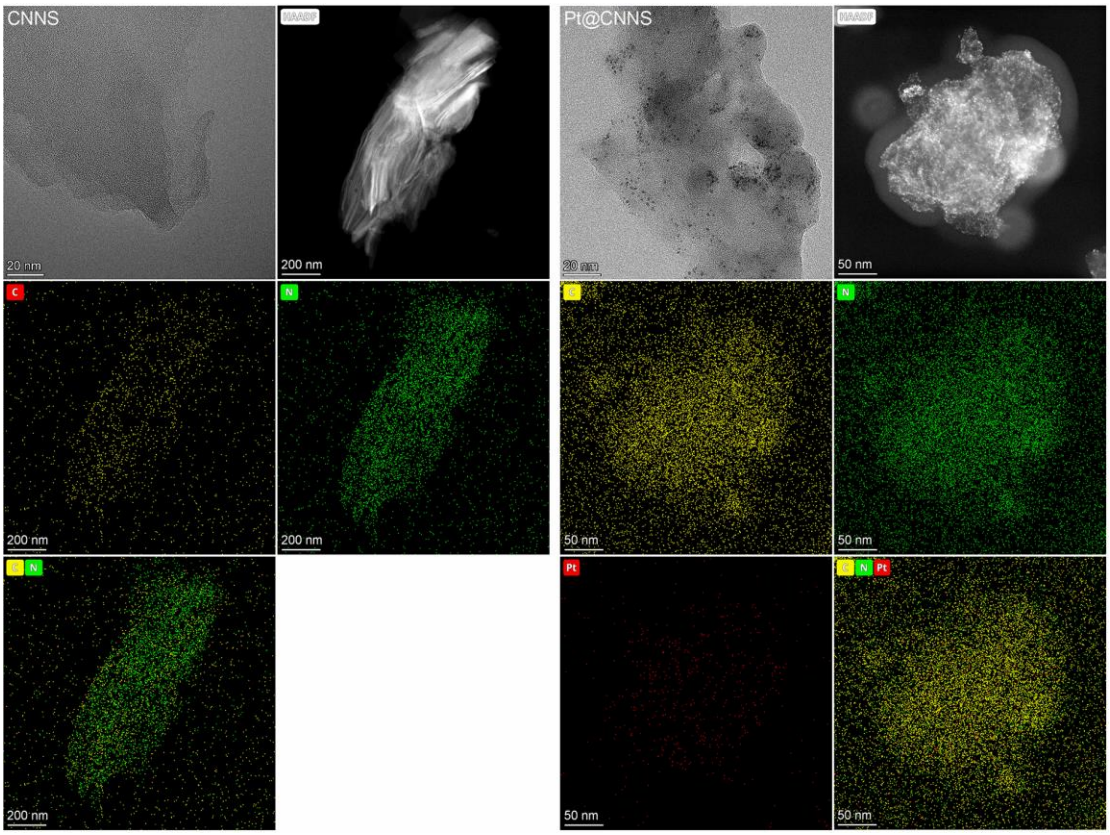

Figure S7. TEM images of CNNS and Pt@CNNS and the corresponding elemental mapping of C, N, and Pt.

Notes: From the above TEM images, some nanoparticles (PtOx) could be identified for Pt@CNNS. Such observation is reasonable, since our synthetic route (CNNS + H_2PtCl_6, 60 °C, 6 h) was similar to Nichols et al. (CNNS + $PtCl_2$/ H_2PtCl_6, 90 °C, 48 h).[5] However, upon comparison between the TEM image and the elemental map of Pt, it is clear that besides the nanoparticles, additional Pt (probably ionic Pt) could also be identified. We think that the ionic Pt was responsible for the enhanced photozymatic activity of CNNS at neutral pH, based on the following considerations:

1. Broadened absorption of Pt@CNNS versus CNNS is typical attributed to MLCT from Pt^{2+} to CNNS;
2. It is possible that the PtOx nanoparticles may also contributed to TMB oxidation, but distinct responses were obtained for Pt@CNNS in the absence and presence of light irradiation (either pH 4 or pH 7).

Section 3. Photozymatic activity of Pt@CNNS

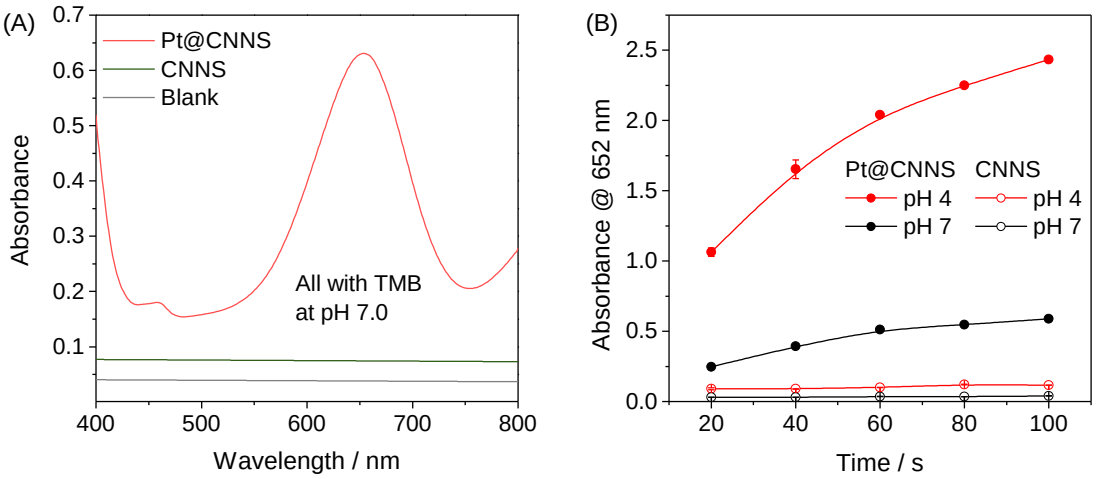

Figure S8. (A) Absorption profiles of TMB after photo-oxidation with CNNS and Pt@CNNS at pH = 7; and (B) time-dependent TMB oxidation with Pt@CNNS and CNNS at pH = 4 and 7.

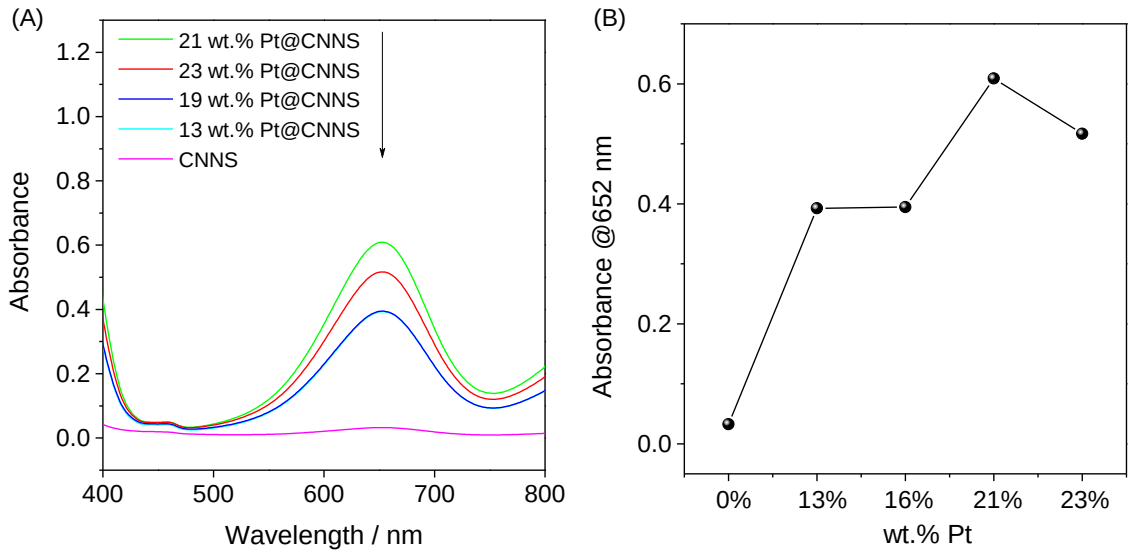

Figure S9. Pt@CNNS oxidized TMB with different Pt doping contents. Experimental conditions: Photozyme: 0.05 mg mL^{-1}; buffer: 20 mM sodium acetate buffer pH 4.0; TMB: 0.8 mM. The final contents of Pt were 2.47% (13%), 2.55% (19%); 3.19% (21%), and 1.05% (23%), respectively.

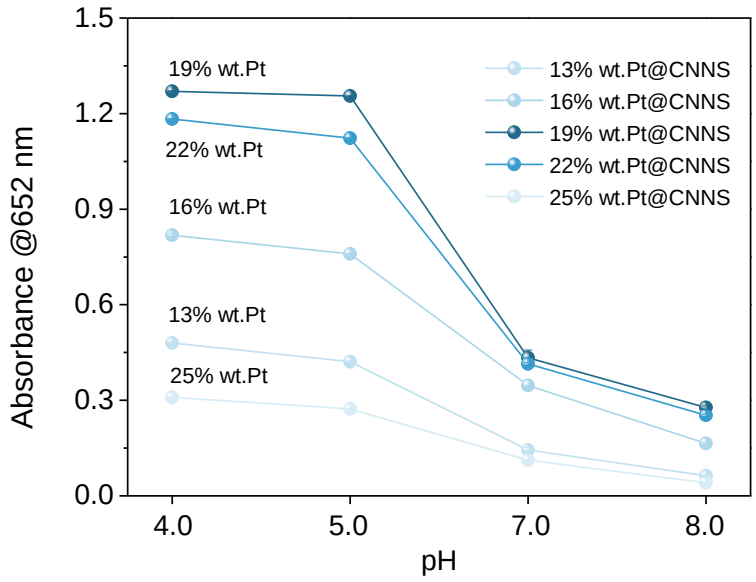

Figure S10. pH-dependent activity of Pt@CNNS (varied Pt contents).

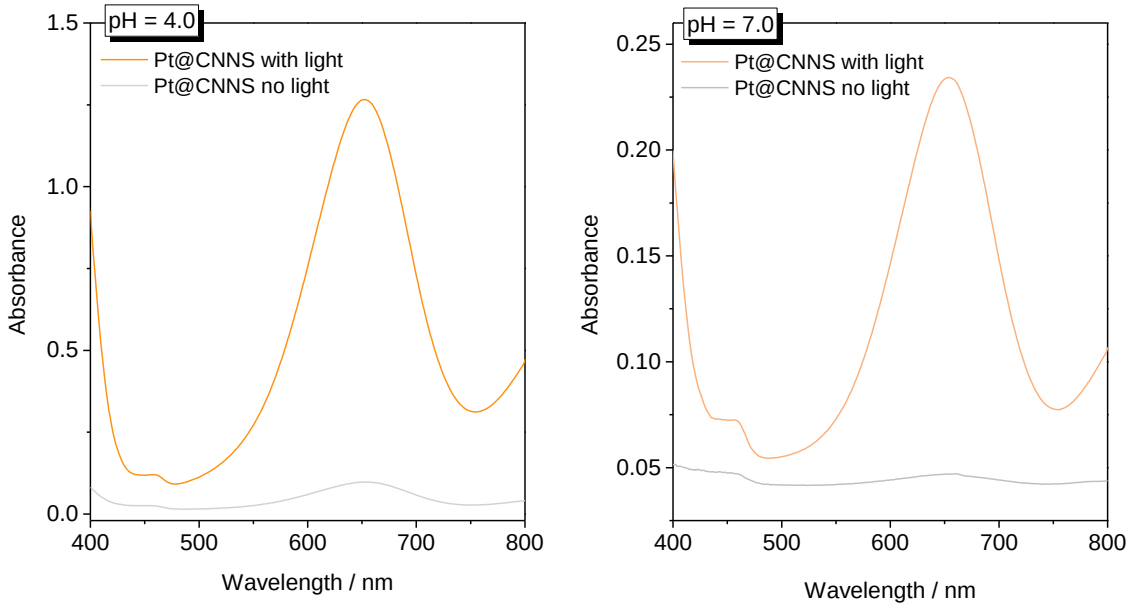

Figure S11. TMB oxidation at pH 4 and 7 in the absence and presence of light.

Notes: As can be evidenced from the TEM images in Figure S7, there are PtOx nanoparticles formed on CNNS. It is possible that the PtOx nanoparticles may also contributed to TMB oxidation, but distinct responses were obtained for Pt@CNNS in the absence and presence of light irradiation (either pH 4 or pH 7). Besides, Broadened absorption of Pt@CNNS versus CNNS is typical attributed to MLCT from Pt^{2+} to CNNS.

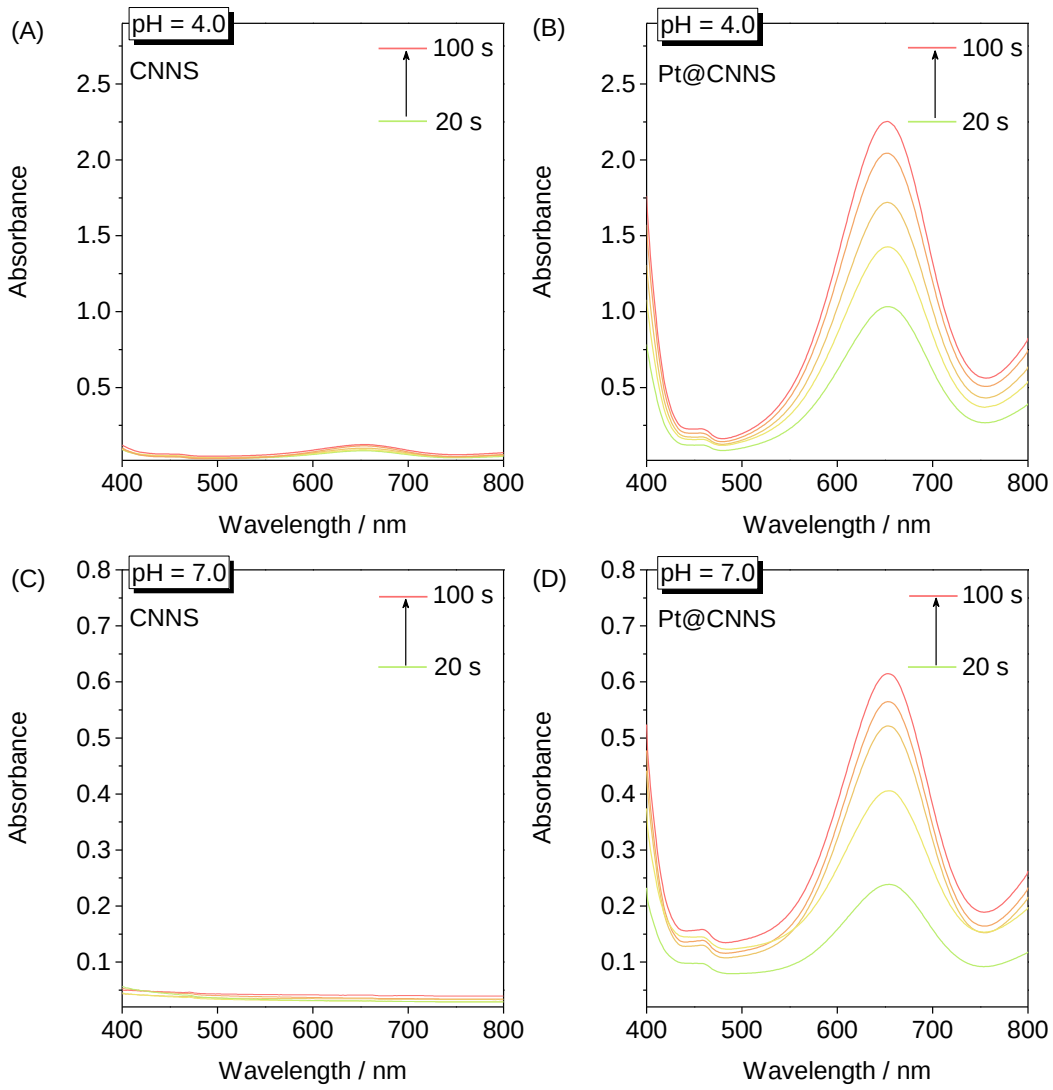

Figure S12. Time-dependent TMB oxidation with CNNS (A and C) and Pt@CNNS (B and D). Experimental conditions: Photozyme: 0.05 mg/mL; buffer: 20 mM sodium acetate buffer pH 4.0; TMB: 0.8 mM.

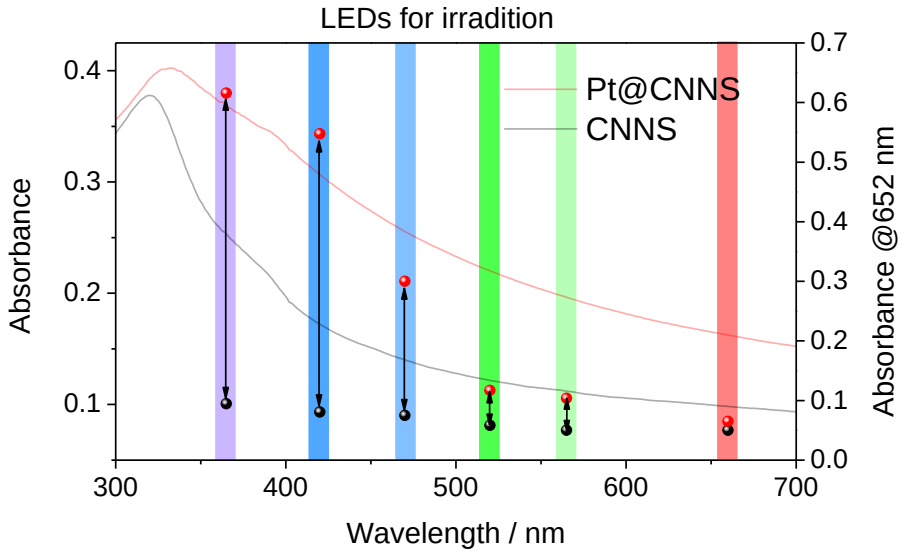

Figure S13. Wavelength-dependent TMB oxidation of Pt@CNNS at neutral pH (pH = 7.0) and CNNS at acidic pH (pH= 4.0). Experimental conditions: Photozyme: 0.05 mg mL^{-1}; buffer: 20 mM sodium acetate buffer pH 7.0 or 4.0; TMB: 0.8 mM.

Notes: The photozymatic performance of the photozyme depends on the wavelength of light absorption (Fig. 1A), so the photo-induced oxidation of TMB by Pt@CNNS and CNNS in the presence of different LEDs (3V, 3W) were compared. As shown in Fig. S13, the oxidation performance results agreed well with the absorbance wavelength.

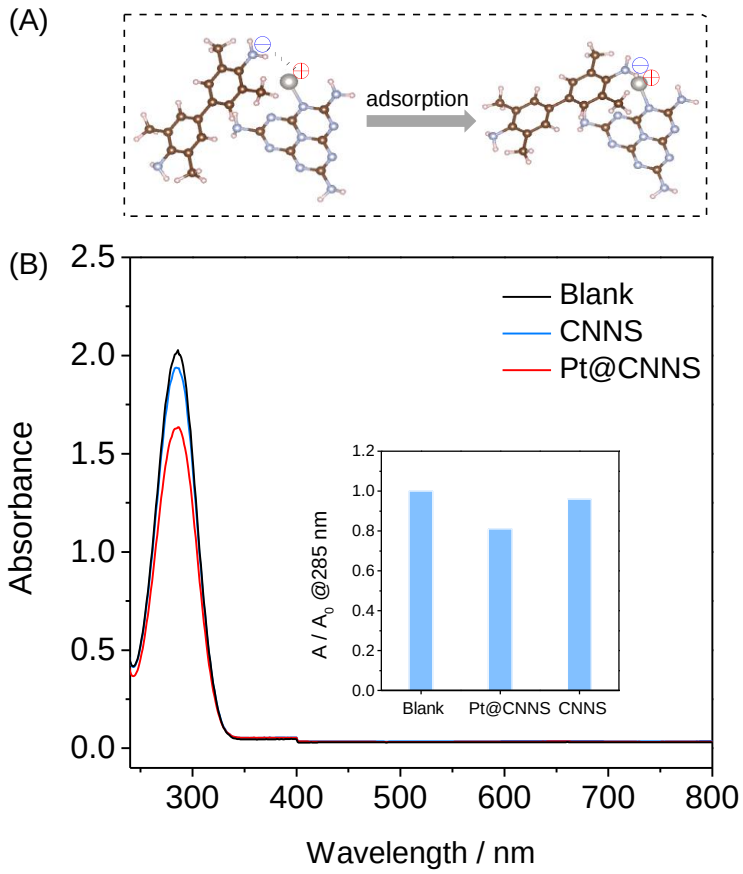

Figure S14. (A) The Schematic of absorption mechanism; (B) the UV-vis absorbance spectra of Pt@CNNS and CNNS with TMB. The inset in figure was the relative intensity of the absorbance.

Notes: For the apparent change of K_m, potential adsorption of Pt@CNNS or CNNS were proposed. In the adsorption process, the electron-rich N- of TMB was attracted to the Pt of Pt@CNNS. As shown in Fig. S14, the TMB absorbance at 288 nm markedly decreased as the nanozyme added, but the absorbance at 652 nm did not appear, suggesting that the decrease at 288 nm was not oxidation-induced.

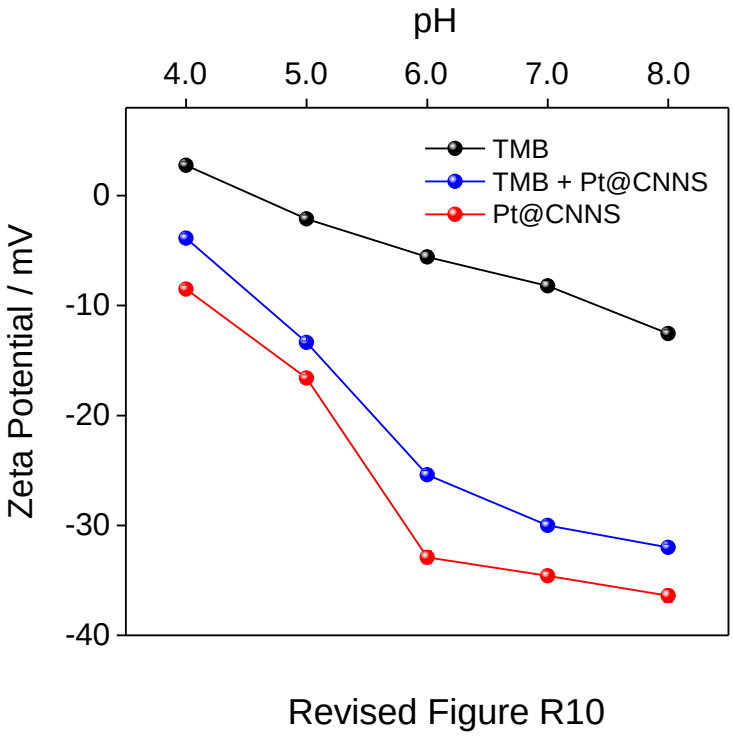

Figure S15. Zeta potentials of TMB, Pt@CNNS, and “TMB + Pt@CNNS” at different pH.

Section 4. Enzymatic kinetics of Pt@CNNS

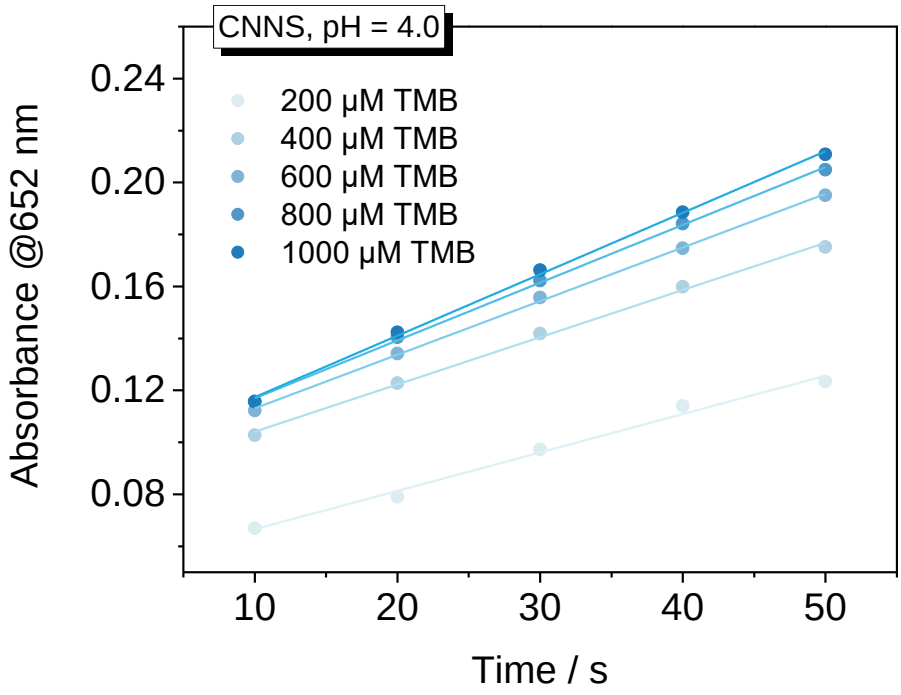

Figure S16. The enzyme-like activity of CNNS at pH 4.

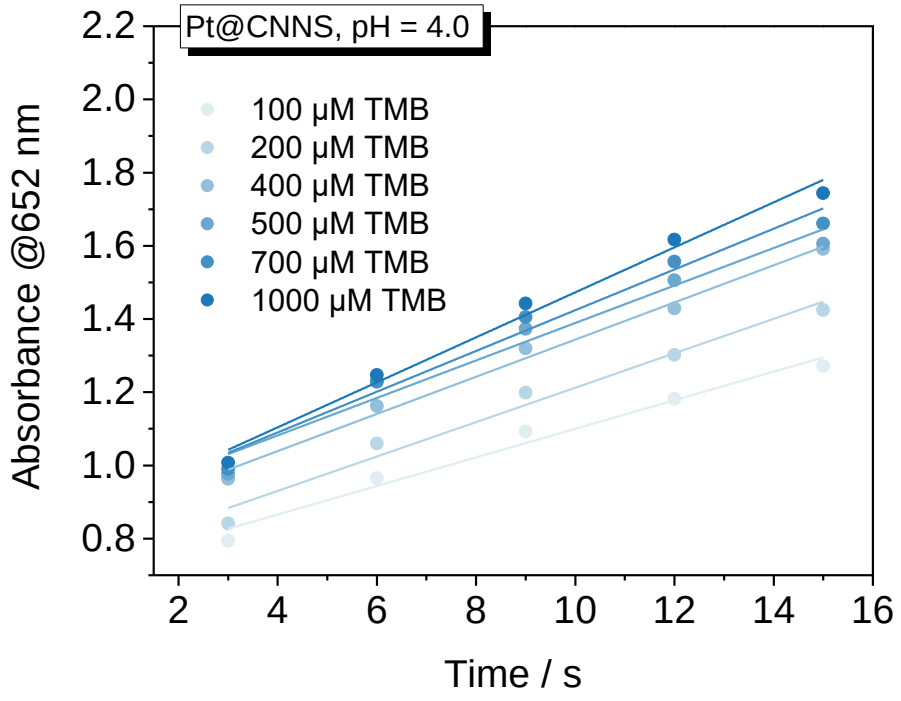

Figure S17. The enzyme-like activity of Pt@CNNS at pH 4.

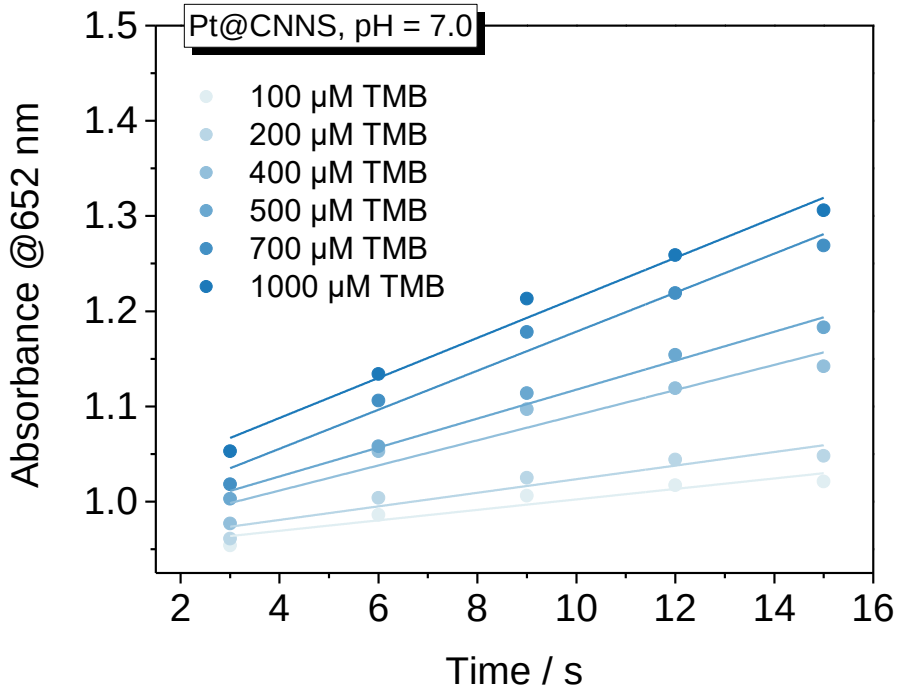

Figure S18. The enzyme-like activity of Pt@CNNS at pH 7.

Section 5. ROS generation from Pt@CNNS

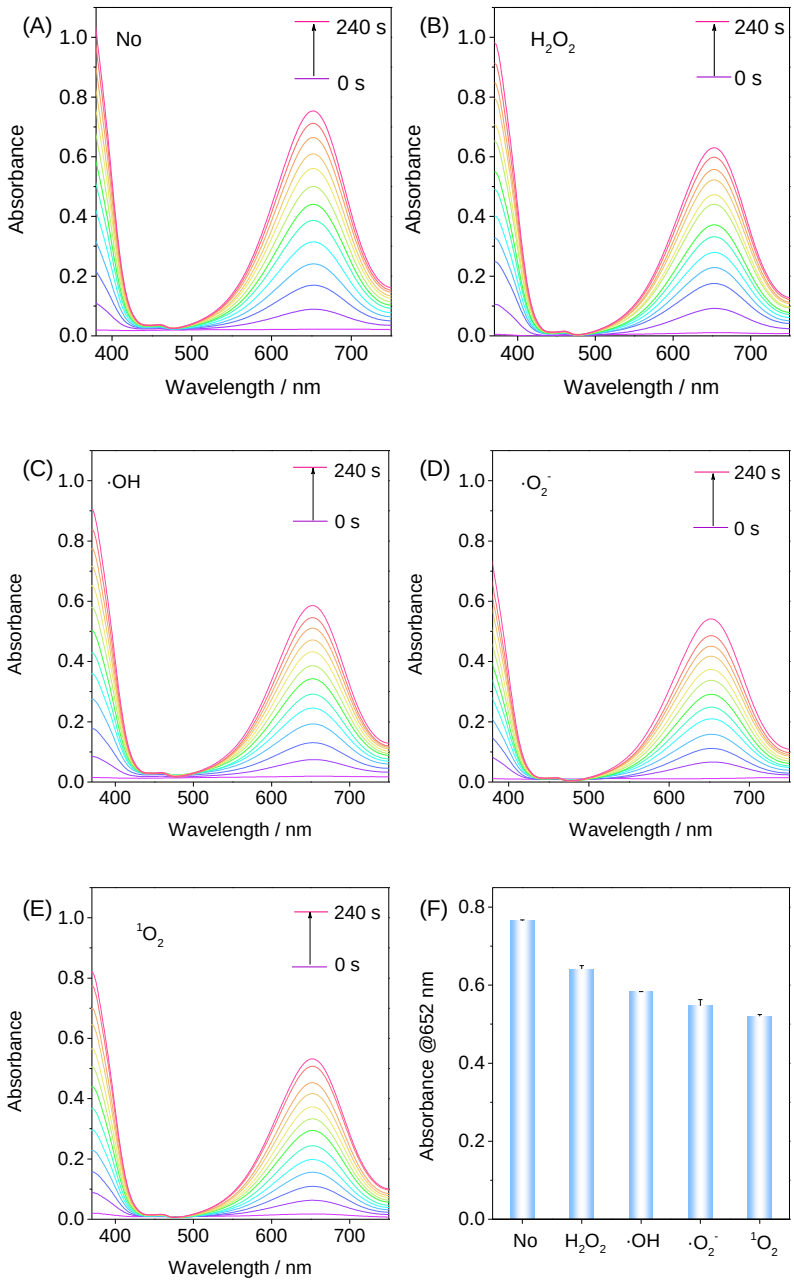

Figure S19. The absorbance of TMB oxidation with Pt@CNNS at pH 4 in the presence of ROS scavengers: (A) No scavengers; (B) catalase; (C) mannite; (D) superoxide dismutase; (E) D-tryptophan. (F) Comparison of the main ROS in the process of TMB oxidation. Experimental conditions: Photozyme: 0.02 mg mL^{-1}; buffer: 20 mM sodium acetate buffer pH 4.0; TMB: 0.8 mM; SOD: 800 U; D-tryptophan: 4.9 mM; catalase: 150 U; mannite: 10.0 mM.

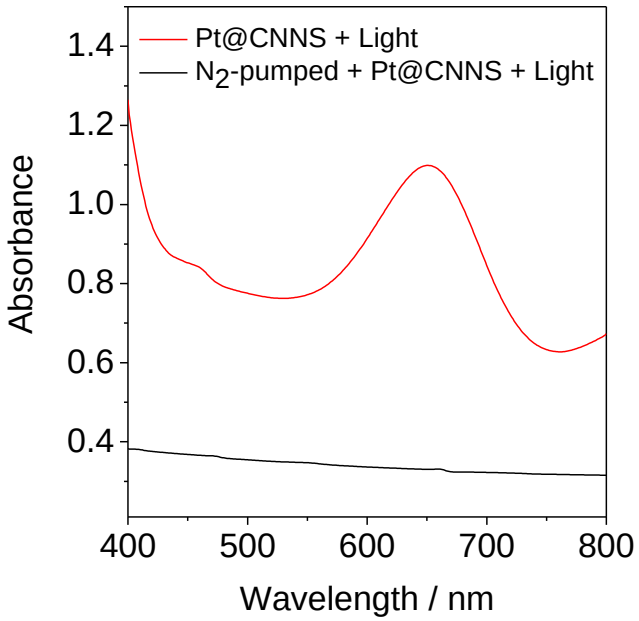

Figure S20. The absorbance spectra of Pt@CNNS with TMB under different conditions.

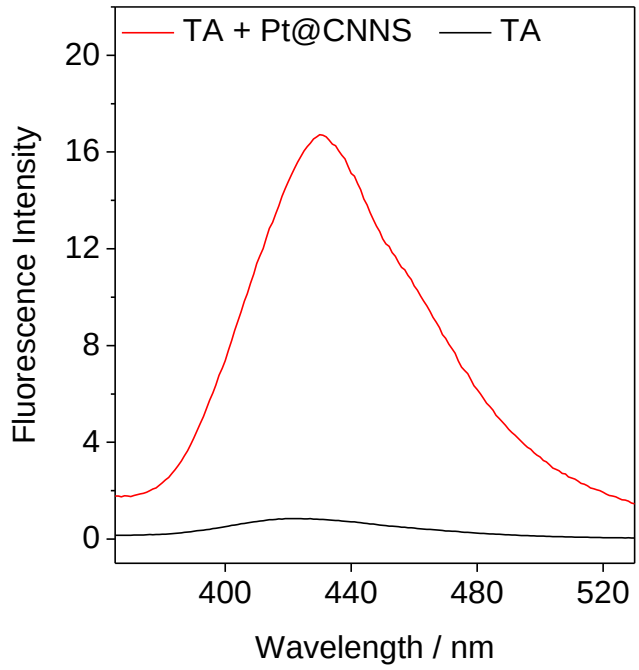

Figure S21. Fluorescence spectra of terephthalate incubated with Pt@CNNS under blue LED irradiation. Experimental conditions: terephthalate (6 mM); buffer: 100 mM sodium acetate buffer pH 7.0.

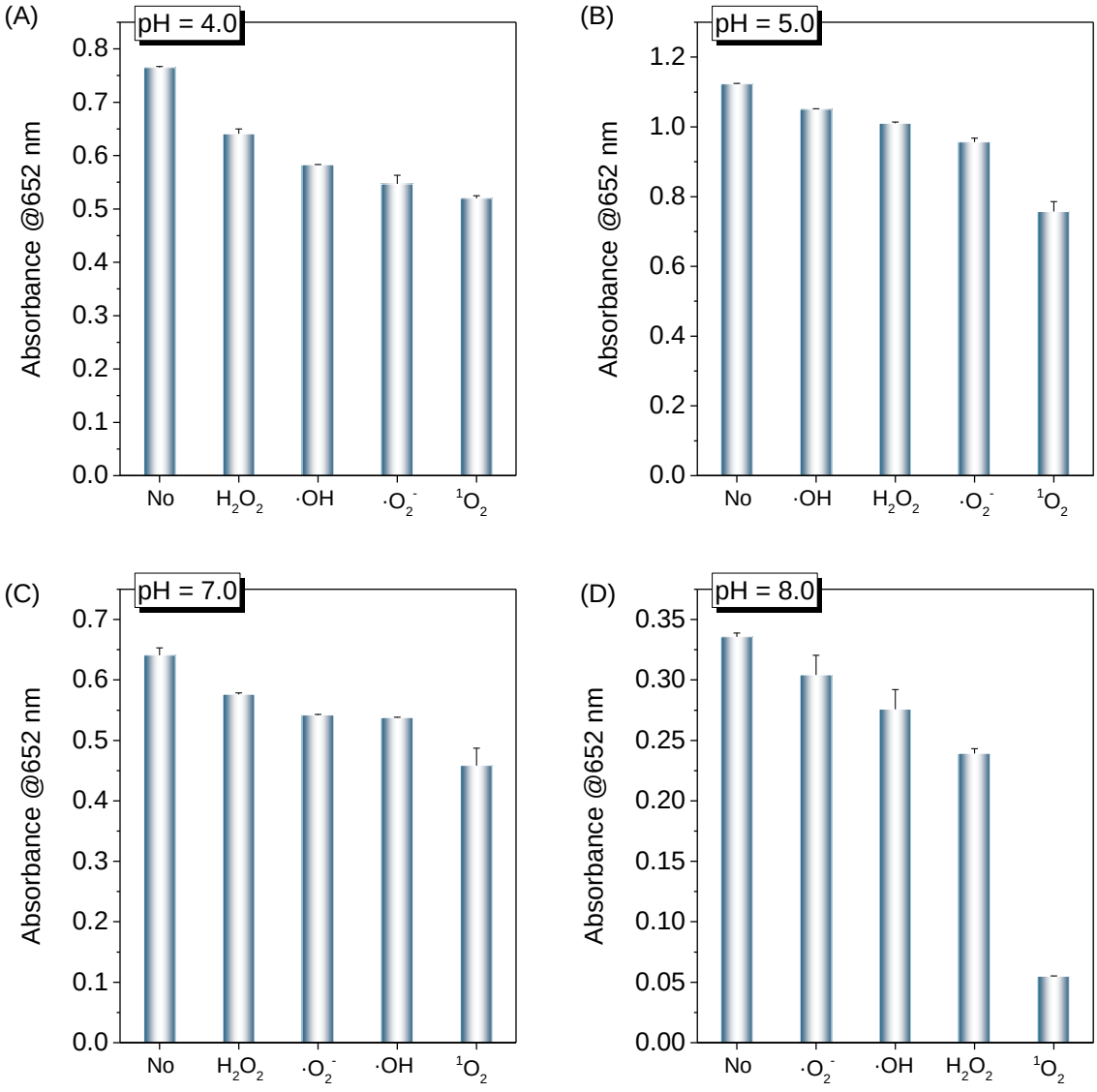

Figure S22. Identification of the specific ROS generated for TMB oxidation at pH 7 through scavenger studies. Experimental conditions: Photozyme: pH 4.0: 0.02 mg mL^{-1}; pH 5.0: 0.03 mg mL^{-1}; pH 7.0-8.0: 0.05 mg mL^{-1}; buffer: 20 mM sodium acetate buffer pH 7.0; TMB: 0.8 mM; SOD: 800 U; D-tryptophan: 4.9 mM; catalase: 150 U; mannite: 10.0 mM.

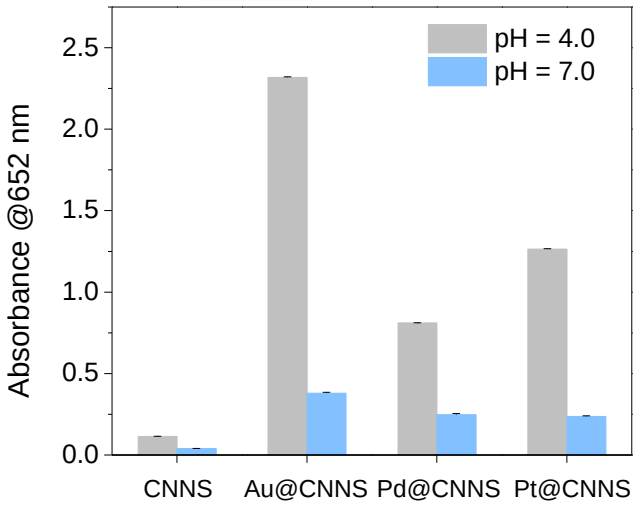

Figure S23. Comparison of the photozymatic activity of CNNS, Pt@CNNS, Au@CNNS, and Pd@CNNS.

Section 6. Colorimetric Determination of Antioxidants

Table S3. Structures of the antioxidants investigated in this work.

(-)-Epigallocatechin gallate (EGCG)	(±)-Catechin hydrate (CT)	Gallic acid (GA)	Ascorbic acid (AA)
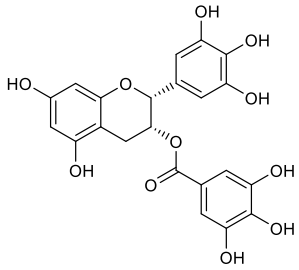	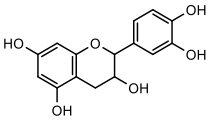	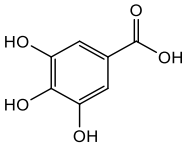	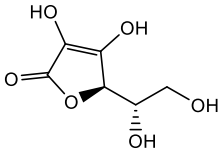
Chlorogenic acid (CHA)	**Caffeic acid (CA)**	**Quercetin (QR)**	**Rutin**
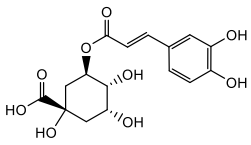	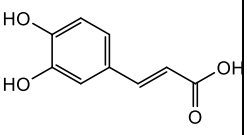	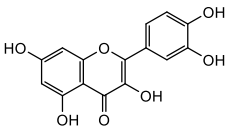	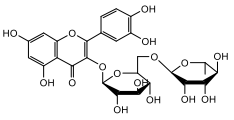

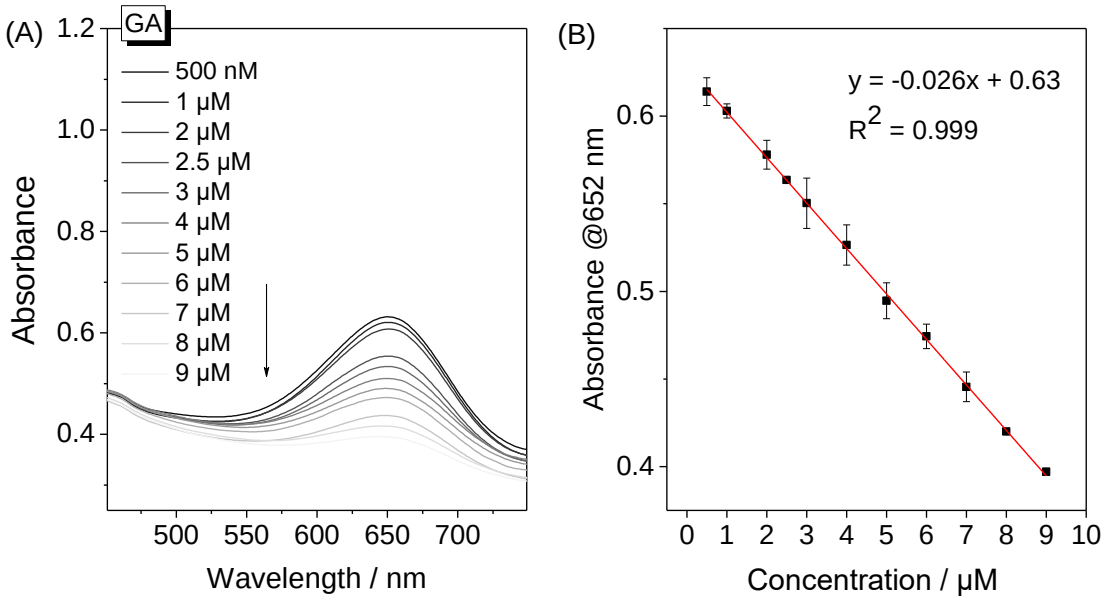

Figure S24. (A) The UV-vis absorbance spectra at different EGCG concentration and the (B) standard calibration curve in colorimetric analysis at pH 7.

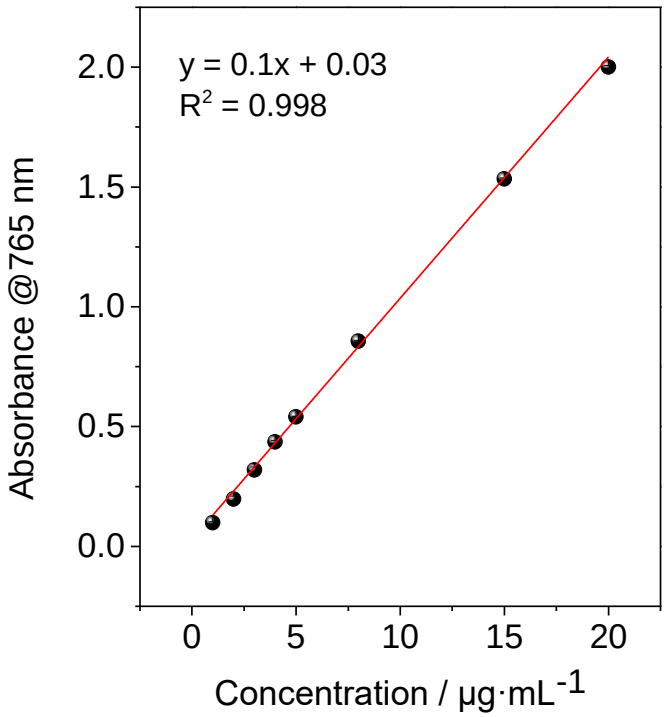

Figure S25. Standard calibration curve of classical Folin-Ciocalteu method.

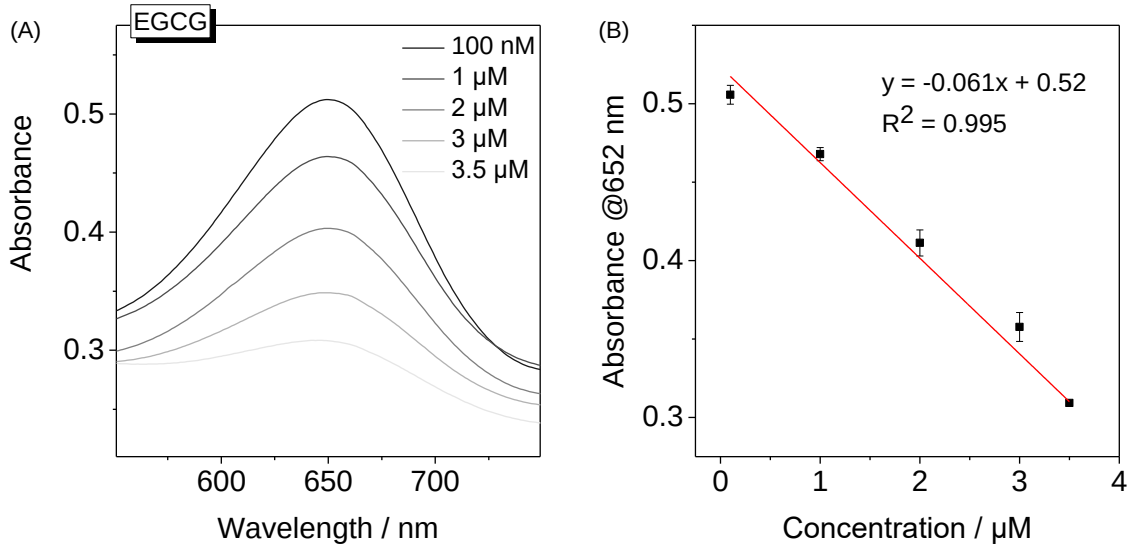

Figure S26. (A) The UV-vis absorbance spectra at different EGCG concentration and (B) the linear curve between absorbance and EGCG concentration.

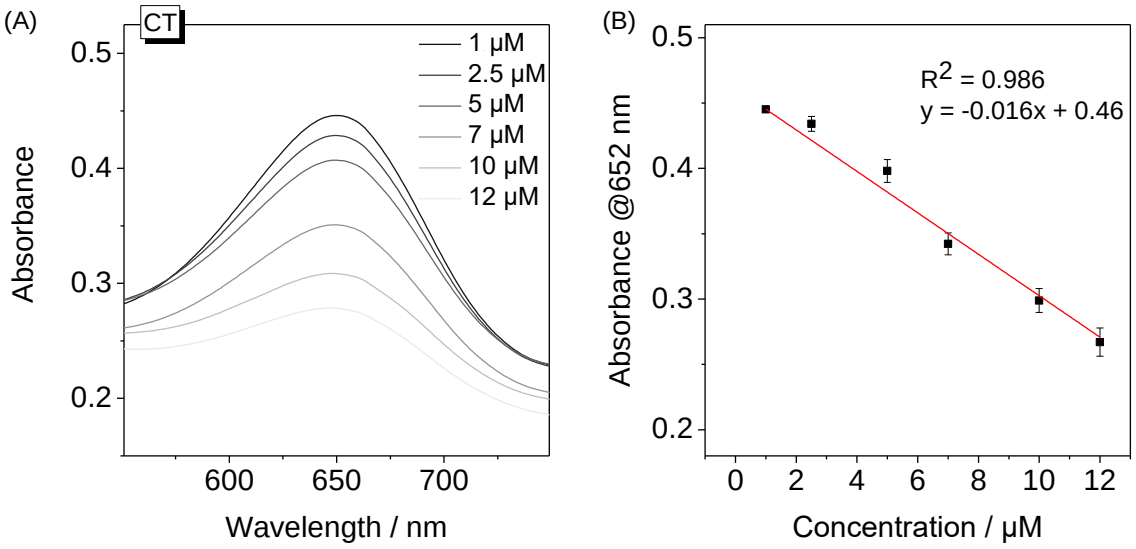

Figure S27. (A) The UV-vis absorbance spectra at different CT concentration and (B) the linear curve between absorbance and CT concentration.

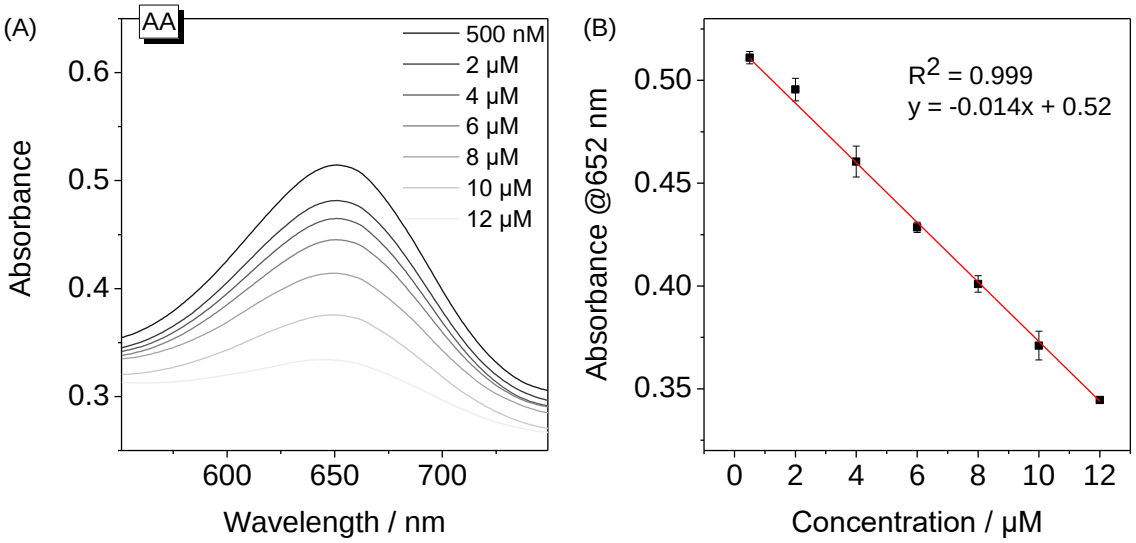

Figure S28. (A) The UV-vis absorbance spectra at different AA concentration and (B) the linear curve between absorbance and AA concentration.

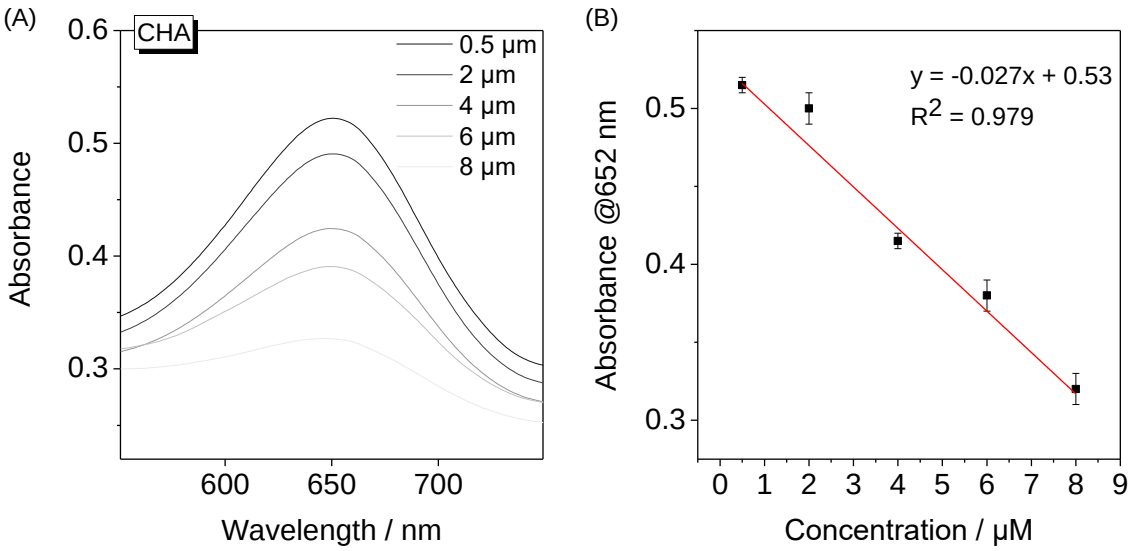

Figure S29. (A) The UV-vis absorbance spectra at different CHA concentration and (B) the linear curve between absorbance and CHA concentration.

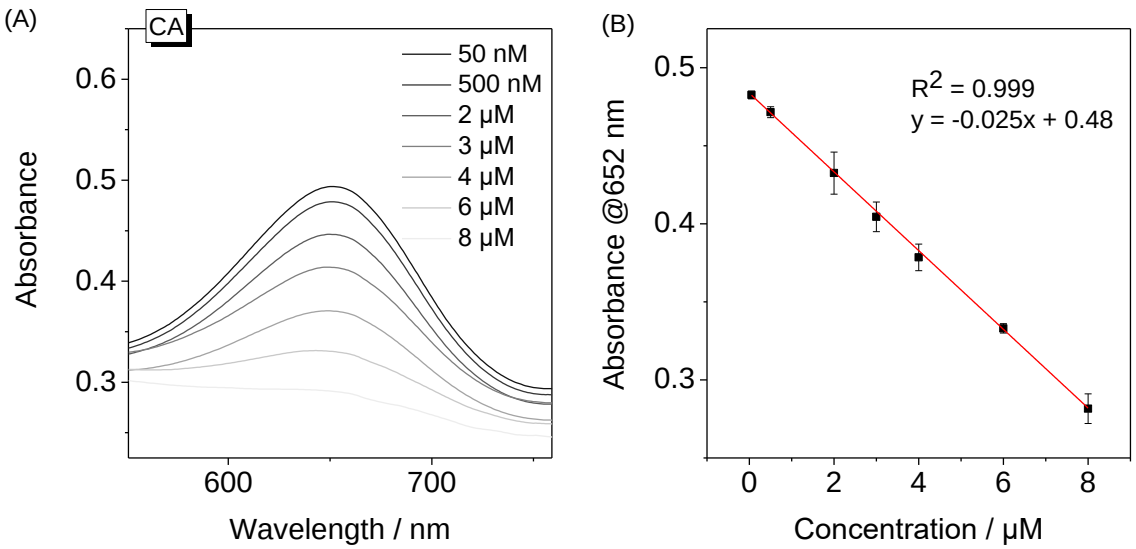

Figure S30. (A) The UV-vis absorbance spectra at different CA concentration and (B) the linear curve between absorbance and CA concentration.

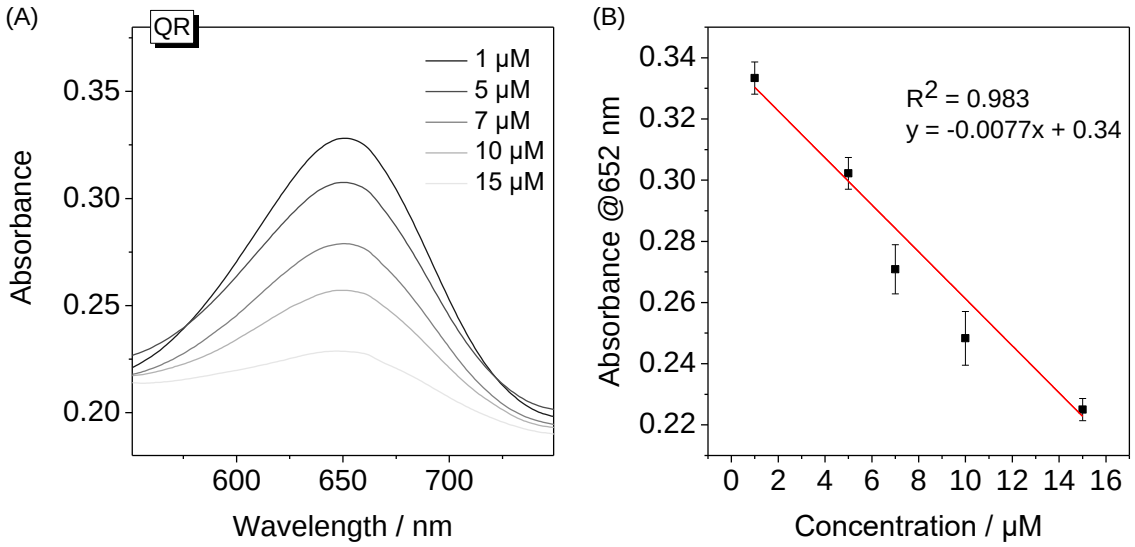

Figure S31. (A) The UV-vis absorbance spectra at different QR concentration and (B) the linear curve between absorbance and QR concentration.

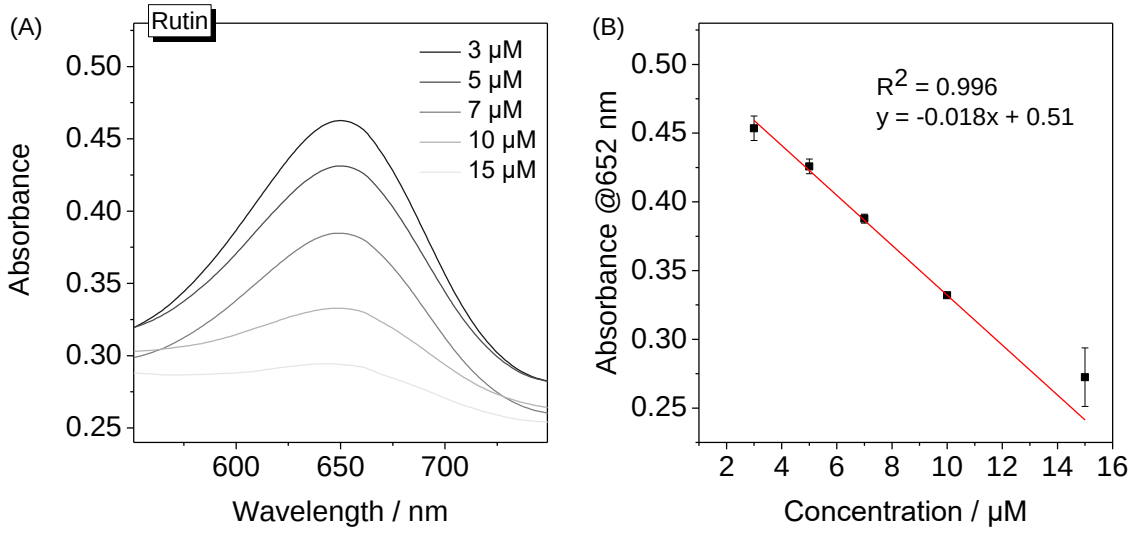

Figure S32. (A) The UV-vis absorbance spectra at different Rutin concentration and (B) the linear curve between absorbance and Rutin concentration.

Table S4. Linear Equations, Correlation Coefficients and Linear Ranges for Antioxidants.

Antioxidants	Linear equation	Linear range (μmol·L^{-1})	R^2
(-)-Epigallocatechin gallate	y = - 0.061x + 0.52	0.10 ~ 3.5	0.995
(±)-Catechin hydrate	y = - 0.016x + 0.46	1.0 ~ 12	0.986
Gallic acid	y = - 0.026x + 0.63	0.50 ~ 9.0	0.999
Ascorbic acid	y = - 0.014x + 0.52	0.50 ~ 12	0.999
Chlorogenic acid	y = - 0.027x + 0.53	0.50 ~ 8.0	0.979
Caffeic acid	y = - 0.025x + 0.48	0.050 ~ 8.0	0.999
Quercetin	y = - 0.0077x + 0.34	1.0 ~ 15	0.983
Rutin	y = - 0.018x + 0.51	3.0 ~ 15	0.996

Section 7. Evaluation of Antioxidants in Tea samples

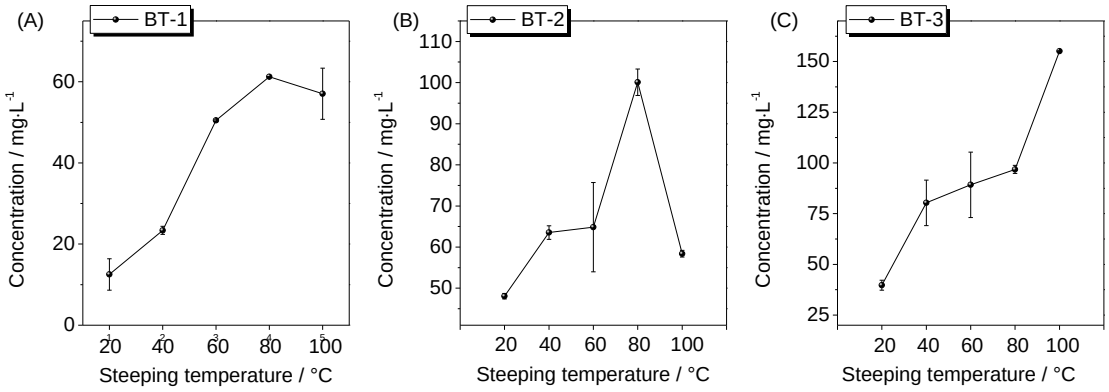

Figure S33. Effect of steeping temperature on antioxidants capacities of each of the three Black Teas (BT).

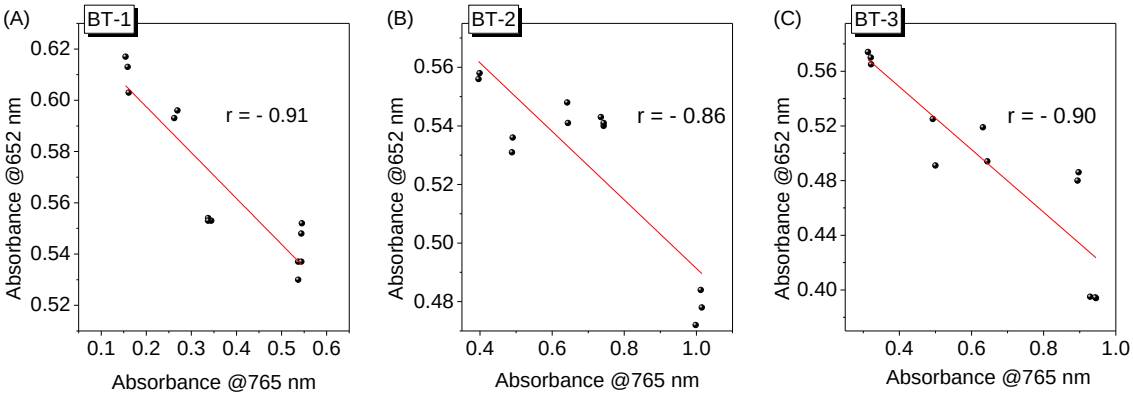

Figure S34. The results of this method and the Folin-Ciocalteu method for the analysis of the effect of steeping temperature on the antioxidant capacities of BT with Bland-Altman analysis.

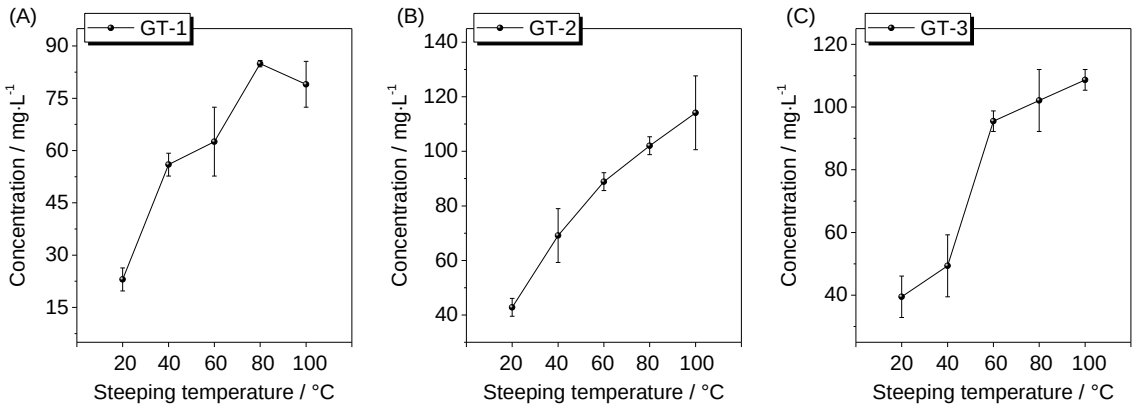

Figure S35. Effect of steeping temperature on antioxidants capacities of each of the three Green Teas (GT).

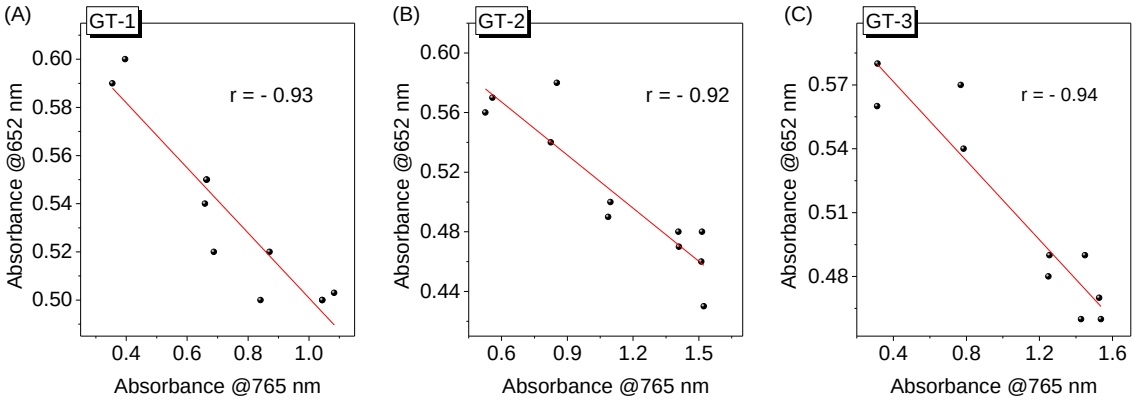

Figure S36. The results of this method and the Folin-Ciocalteu method for the analysis of the effect of steeping temperature on the antioxidant capacities of GT with Bland-Altman analysis.

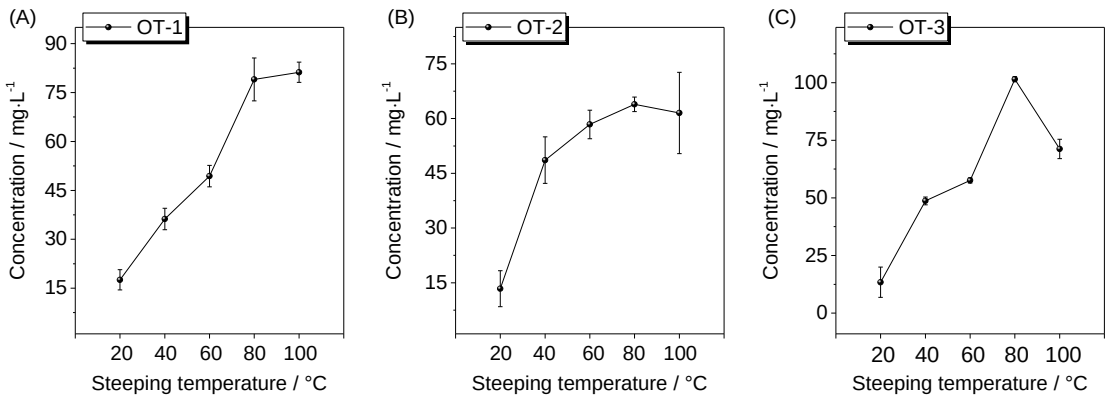

Figure S37. Effect of steeping temperature on antioxidants capacities of each of the three Oolong Teas (OT).

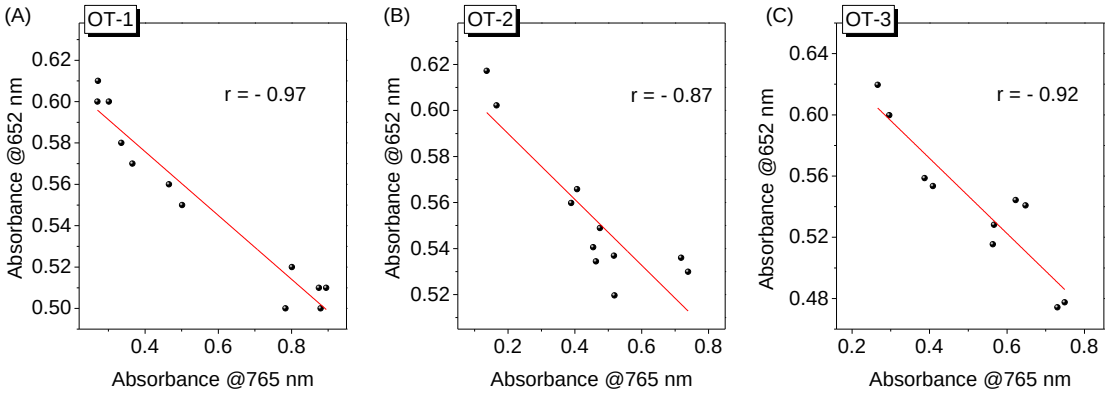

Figure S38. The results of this method and the Folin-Ciocalteu method for the analysis of the effect of steeping temperature on the antioxidant capacities of OT with Bland-Altman analysis.

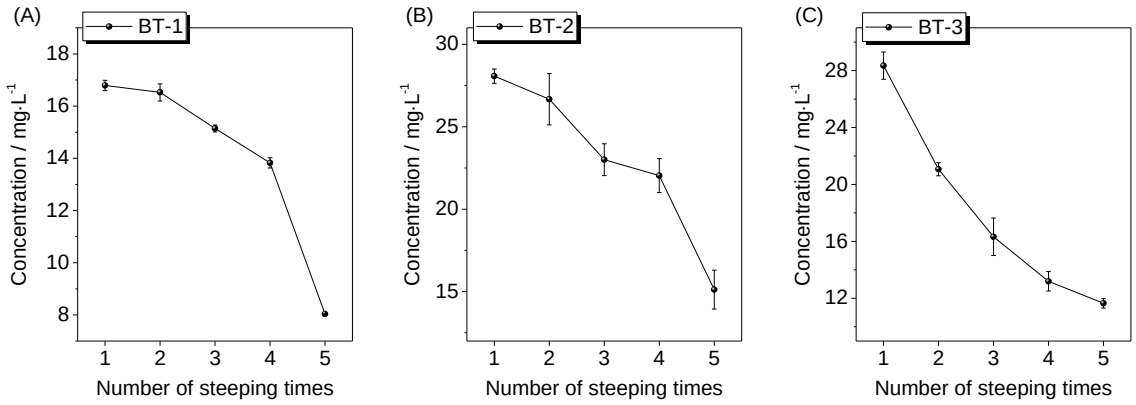

Figure S39. Effect of steeping times on antioxidants capacities of each of the three Black Teas (BT).

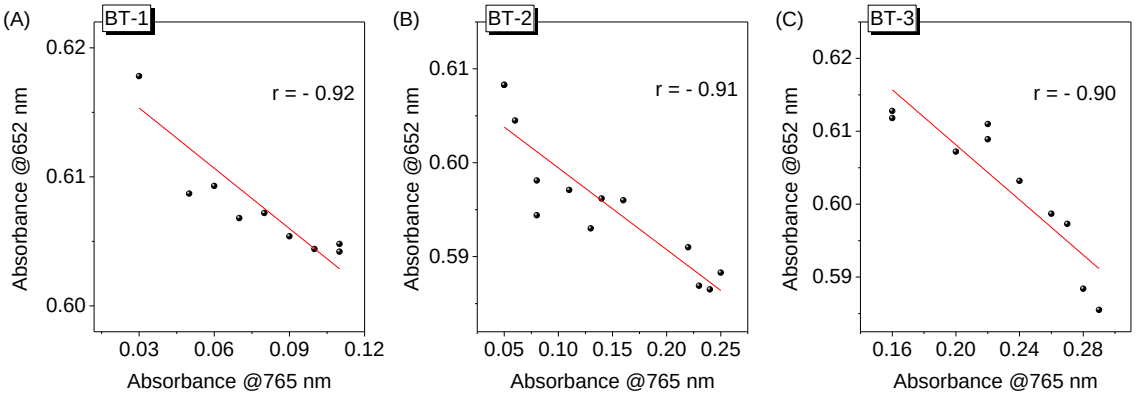

Figure S40. The results of this method and the Folin-Ciocalteu method for the analysis of the effect of steeping times on the antioxidant capacities of BT with Bland-Altman analysis.

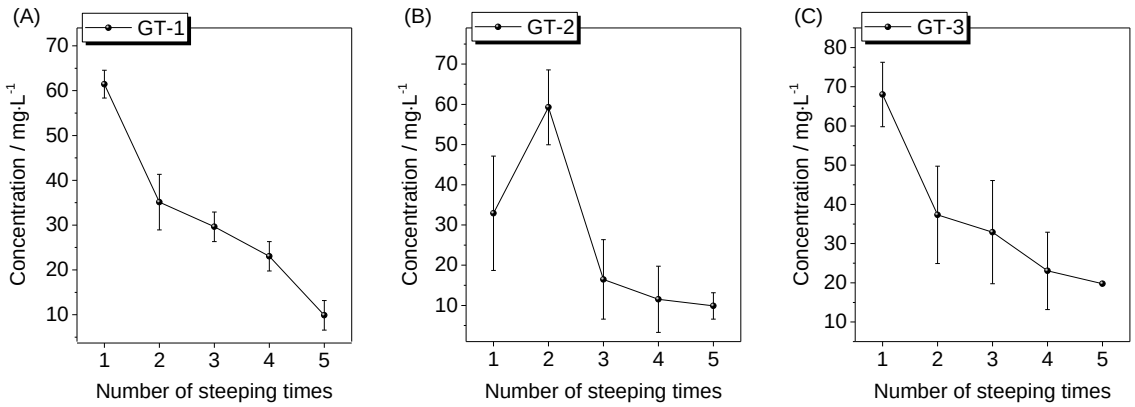

Figure S41. Effect of steeping times on antioxidants capacities of each of the three Green Teas (GT).

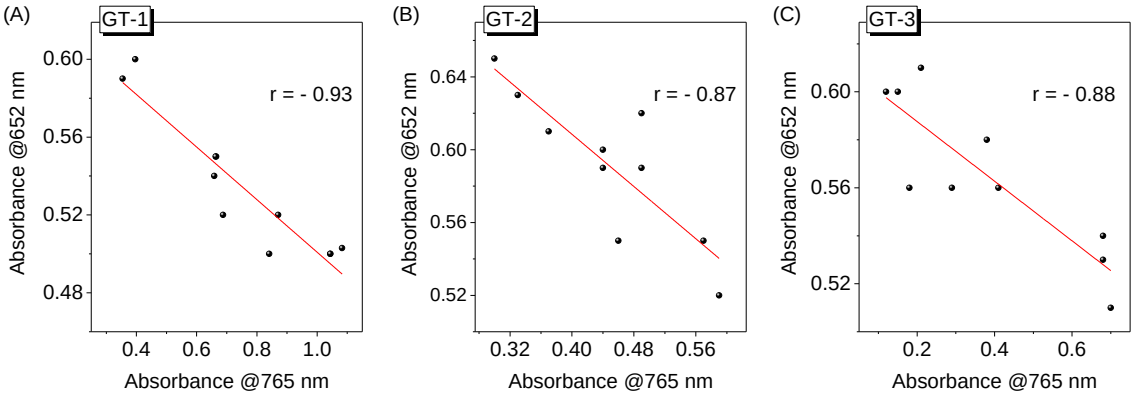

Figure S42. The results of this method and the Folin-Ciocalteu method for the analysis of the effect of steeping times on the antioxidant capacities of GT with Bland-Altman analysis.

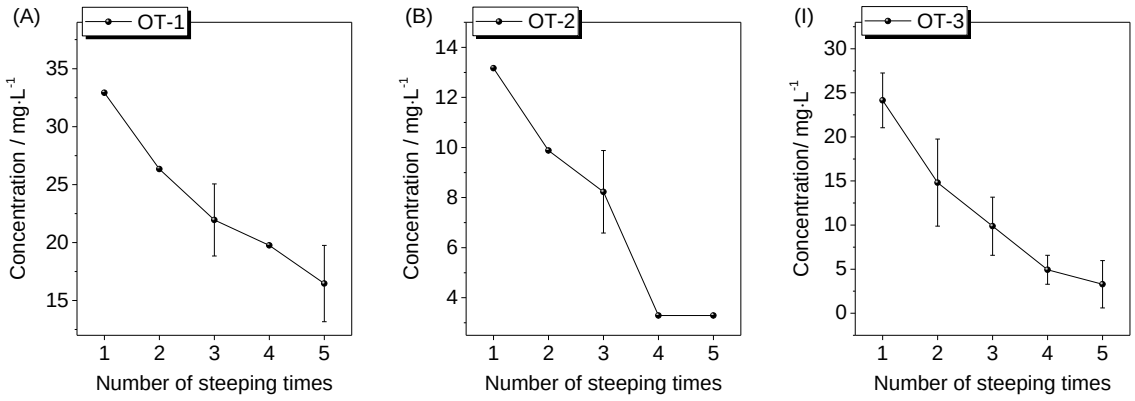

Figure S43. Effect of steeping times on antioxidants capacities of each of the three Oolong Teas (OT).

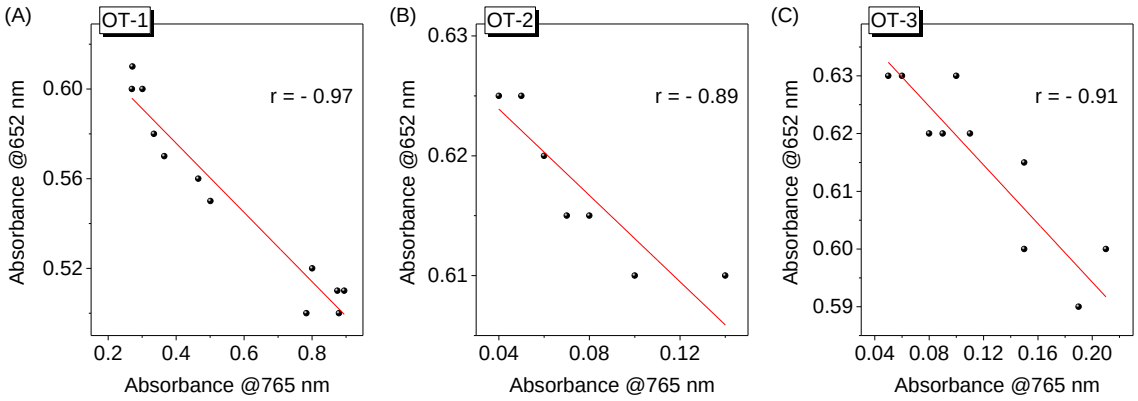

Figure S44. The results of this method and the Folin-Ciocalteu method for the analysis of the effect of steeping times on the antioxidant capacities of OT with Bland-Altman analysis.

Table S5. Effect of steeping temperature on antioxidants capacities of teas as found with our method and the Folin–Ciocalteu method.

Samples	Colorimetric at neutral pH (mg L^{-1})					Folin-Ciocalteu method (mg L^{-1})					r
Temperature (ºC)	20	40	60	80	100	20	40	60	80	100	
BT1	12.50 ± 3.88	23.38 ± 0.99	50.48 ± 0.31	61.24	57.01 ± 6.30	12.80 ± 0.29	23.55 ± 0.35	30.93 ± 0.33	51.05 ± 0.35	51.20 ± 0.36	- 0.91
BT2	48.07 ± 0.66	63.54 ± 1.65	64.86 ± 10.86	100.08 ± 3.22	58.38 ± 0.82	36.75 ± 0.15	46.00 ± 0.10	61.30 ± 0.10	97.83 ± 0.74	71.03 ± 0.38	- 0.86
BT3	39.73 ± 2.42	80.33 ± 11.19	89.22 ± 16.13	96.79 ± 1.98	155.07 ± 0.27	28.87 ± 0.40	46.65 ± 0.35	60.80 ± 0.60	86.55 ± 0.15	90.90 ± 0.71	- 0.90
GT1	23.05 ± 3.29	55.97 ± 3.29	62.55 ± 9.88	84.94 ± 0.93	79.02 ± 6.58	35.54 ± 2.08	63.18 ± 0.31	64.57 ± 1.22	102.69 ± 1.85	82.60 ± 8.94	- 0.93
GT2	42.80 ± 3.29	69.14 ± 9.88	88.89 ± 3.29	102.06 ± 3.29	114.13 ± 13.53	51.22 ± 1.65	80.88 ± 1.36	106.17 ± 0.54	137.81 ± 0.09	148.62 ± 0.48	- 0.92
GT3	39.51 ± 6.58	49.38 ± 9.88	95.47 ± 3.29	102.06 ± 9.88	108.65 ± 3.29	28.26 ± 0.13	74.73 ± 0.76	122.22 ± 0.29	140.86 ± 1.11	150.22 ± 0.49	- 0.94
OT1	17.56 ± 3.10	36.22 ± 3.29	49.38 ± 3.29	79.00 ± 6.58	81.21 ± 3.10	25.10 ± 1.43	38.82 ± 1.53	60.32 ± 1.79	76.23 ± 0.86	85.31 ± 0.86	- 0.97
OT2	13.37 ± 4.94	48.62 ± 6.38	58.41 ± 3.91	63.90 ± 2.01	61.53 ± 11.16	12.11 ± 1.48	36.69 ± 0.75	43.48 ± 0.83	69.89 ± 1.03	48.81 ± 0.07	- 0.87
OT3	13.40 ± 6.55	48.69 ± 1.68	57.58 ± 1.15	101.50 ± 1.09	71.25 ± 4.21	25.14 ± 1.49	36.81 ± 1.07	60.53 ± 1.28	70.96 ± 0.95	53.51 ± 0.17	- 0.92

Table S6. Effect of steeping times on antioxidants capacities of teas as found with our method and the Folin–Ciocalteu method.

Samples	Colorimetric at neutral pH (mg L^{-1})					Folin-Ciocalteu method (mg L^{-1})					r
Steeping times	1	2	3	4	5	1	2	3	4	5	
BT1	16.79 ± 0.20	16.53 ± 0.33	15.14 ± 0.13	13.83 ± 0.20	8.03	7.50 ± 0.50	5.50 ± 0.50	3.50 ± 0.50	2.50 ± 0.50	0.50 ± 0.50	- 0.92
BT2	28.07 ± 0.43	26.67 ± 1.55	23.00 ± 0.96	22.03 ± 1.03	15.12 ± 1.18	20.67 ± 0.94	19.67 ± 0.94	11.33 ± 1.25	6.00 ± 1.41	2.33 ± 0.47	- 0.91
BT3	28.35 ± 0.95	21.07 ± 0.46	16.33 ± 1.32	13.20 ± 0.69	11.65 ± 0.33	25.50 ± 0.50	23.50 ± 0.50	19.00 ± 2.00	19.00	13.00	- 0.90
GT1	61.46 ± 3.10	35.12 ± 6.28	29.63 ± 3.29	23.05 ± 3.29	9.88 ± 3.29	61.46 ± 0.94	37.67 ± 0.94	23.00	15.00	12.00 ± 1.00	- 0.93
GT2	32.92 ± 14.22	59.26 ± 9.13	16.46 ± 9.88	11.52 ± 8.23	9.88 ± 3.29	41.67 ± 0.94	54.67 ± 0.94	46.00	34.00	28.50 ± 1.50	- 0.87
GT3	68.04 ± 8.21	37.31 ± 12.42	32.92 ± 13.17	23.05 ± 9.88	19.76	65.67 ± 0.94	36.50 ± 1.50	27.50 ± 1.50	16.00 ± 1.41	10.00 ± 1.41	- 0.88
OT1	32.92	26.34	21.95 ± 3.10	19.75	16.46 ± 3.29	28.67 ± 0.94	22.00	13.00 ± 1.41	8.33 ± 1.89	8.00 ± 1.00	- 0.97
OT2	13.17	9.88	8.23 ± 1.65	3.29	3.29	9.00 ± 2.00	4.50 ± 0.50	3.50 ± 0.50	2.00	1.00	- 0.89
OT3	24.14 ± 3.10	14.82 ± 4.94	9.87 ± 3.29	4.94 ± 1.65	3.29 ± 2.67	16.67 ± 0.94	12.00	7.00 ± 1.00	6.50 ± 0.50	3.33 ± 1.25	- 0.91

References

1 J. Y. Zhang, S. H. Wu, X. M. Lu, P. Wu and J. W. Liu, *Nano Lett.*, 2019, **19**, 3214.

2 S. H. Wu, R. H. Zhou, H. J. Chen, J. Y. Zhang and P. Wu, *Nanoscale*, 2020, **12**, 5543.

3 S. C. Yan, Z. S. Li and Z. G. Zou, *Langmuir*, 2009, **25**, 10397.

4 S. Tonda, S. Kumar, S. Kandula and V. Shanker, *J. Mater. Chem. A*, 2014, **2**, 6772.

5 F. Nichols, J. E. Lu, R. Mercado, R. Dudschus, F. Bridges and S. W. Chen, *Chem. Eur. J.*, 2020, **26**, 4136.